

**DOKUZ EYLÜL UNIVERSITY**  
**GRADUATE SCHOOL OF NATURAL AND APPLIED**  
**SCIENCES**

**HUMAN GAIT ANALYSIS AND WALKING**  
**PATTERN GENERATOR**

**by**

**Gökmen AŞCIOĞLU**

**January, 2014**

**İZMİR**

# **HUMAN GAIT ANALYSIS AND WALKING PATTERN GENERATOR**

**A Thesis Submitted to the**

**Graduate School of Natural and Applied Sciences of Dokuz Eylül  
University**

**In Partial Fulfilment of the Requirements for the Degree of Master of  
Science in Electrical and Electronics Engineering**

**by**

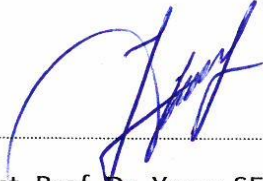
**Gökmen AŞCIOĞLU**

**January, 2014**

**İZMİR**

## THESIS EXAMINATION RESULT FORM

We have read the thesis entitled “HUMAN GAIT ANALYSIS AND WALKING PATTERN GENERATOR” completed by GÖKMEN AŞCIOĞLU under supervision of ASST. PROF. DR. YAVUZ ŞENOL and we certify that in our opinion it is fully adequate, in scope and in quality, as a thesis for the degree of Master of Science.

  
Asst. Prof. Dr. Yavuz ŞENOL

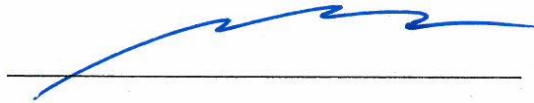
Supervisor

  
Asst. Prof. Dr. Ahmet OKUR

(Jury Member)

  
Assoc. Prof. Dr. M. Eren TOYGAR

(Jury Member)

  
Prof. Dr. Ayşe OKUR

Director

Graduate School of Natural and Applied Sciences

## ACKNOWLEDGEMENTS

I would like to express my sincere gratitude to my advisor Asst. Prof. Dr. Yavuz ŞENOL who never lost his faith in me and always supported me through my best and worst days without forgetting his mission to lead me through the way of science and research.

I would like to thank for the mechanical skeleton system designed as part of the TUBITAK Project 110M063 by Dokuz Eylul University Mechanical Engineer Department and Electrical and Electronics Engineering Department.

I would also like to thank my family for their belief in me and their support.

Last but not the least, I wish to thank my colleague, Alican ESLEK, for helping about collection of data for this thesis.

Gökmen AŞCIOĞLU

# HUMAN GAIT ANALYSIS AND WALKING PATTERN GENERATOR

## ABSTRACT

Nowadays, human gait analysis is one of the popular topics and there are many currently available studies. One of the most popular subjects is lower limb prostheses and orthosis in lower extremity which help patients with problems to achieve normal life. Our study has focused on a new method for prediction of gait angles and detection of gait patterns performed in the lower extremity using neural networks with inputs from ground reaction forces and joint angles. In this study, different types of gait patterns including ascending and descending stair have been used and evaluated.

In this thesis, artificial neural networks were used for prediction of gait angles and gait patterns. To predict gait angles and detection of gait patterns artificial neural networks were trained with data sets obtained from joint angles or both joint angles and ground reaction forces. For both cases various type and size of artificial neural networks were trained to provide performance comparison. To provide a useful comparison the results were given in tables.

The performed analyzes has shown that the applied methods have provide acceptable results. Finally these results suggest that neural networks could be applied successfully in prediction of gait angles and the detection of gait patterns.

**Keywords:** Gait analysis, artificial neural networks, gait patterns

# İNSAN YÜRÜYÜŞ ANALİZİ VE YÜRÜME PATTERN ÜRETİMİ

## ÖZ

Günümüzde, insan yürüyüş analizi popüler konulardan biridir ve bu konuda çok sayıda mevcut çalışma bulunmaktadır. En popüler çalışma konularından biri de, alt ekstremitte bölgesinde sorunu olan hastaların normal bir hayat geçirmesine yardım eden alt ekstremitte protezleri ve ortezleridir. Bizim çalışmamız eklem açıları ve yer tepki kuvvetleri girişleriyle yapay sinir ağlarını kullanarak alt ekstremitte bölgesinde gerçekleşen yürüme şekillerinin ve yürüme açılarının tahmini için yeni bir yöntem üzerine odaklanmaktadır. Bu çalışmada; merdiven inme ve çıkma gibi farklı türde yürüme şekilleride kullanılmaktadır ve değerlendirilmektedir.

Bu tezde, yürüme şekillerinin ve yürüme açılarının tahmininde yapay sinir ağları kullanıldı. Yürüme açılarının tahmini ve yürüme şekillerinin tespiti için oluşturulan yapay sinir ağları; eklem açıları ya da hem eklem açıları hem de yer tepki kuvvetlerinden elde edilen veri setleri ile eğitildi. Çeşitli tür ve büyüklükte yapay sinir ağları performans karşılaştırmalarını sağlamak için eğitildi. Kullanışlı bir karşılaştırma sağlamak için sonuçlar tablolar halinde verildi.

Yapılan analizler, tahmin için uygulanan yöntemlerin kabul edilebilir sonuçlar sağladığını gösterir. Bu sonuçlarda son olarak, yapay sinir ağlarının yürüme şekillerinin tespiti ve yürüme açılarının tahmini için başarıyla uygulanabileceğini öne sürer.

**Anahtar Sözcükler:** Yürüme analizi, yapay sinir ağları, yürüme şekilleri

## CONTENTS

	<b>Page</b>
THESIS EXAMINATION RESULT FORM .....	ii
ACKNOWLEDGEMENTS .....	iii
ABSTRACT .....	iv
ÖZ .....	v
LIST OF FIGURES .....	ix
LIST OF TABLES .....	xii
<b>CHAPTER ONE - INTRODUCTION .....</b>	<b>1</b>
1.1 Introduction .....	1
1.2 Thesis Outline.....	2
<b>CHAPTER TWO - GAIT ANALYSIS.....</b>	<b>3</b>
2.1 Introduction .....	3
2.2 Gait Parameters .....	4
2.3 Gait Cycle.....	5
2.3.1 Gait Phases.....	5
2.3.1.1 Rancho Los Amigos Terminology.....	6
2.4 Sensors for Gait Analysis .....	7
2.5 Gait Analysis Methods .....	9
<b>CHAPTER THREE - ARTIFICIAL NEURAL NETWORKS .....</b>	<b>11</b>
3.1 The Biological Model.....	11
3.2 Basic Elements of Artificial Neuron Model.....	12
3.3 Learning Rules in Neural Networks .....	13
3.4 Types of Activation Functions .....	14
3.4.1 Log-Sigmoid Activation Function.....	14
3.4.2 Hyperbolic Tangent Sigmoid Activation Function .....	15

3.4.3 Linear Activation Function.....	16
3.5 Network Architectures .....	16
3.5.1 Multilayer Feedforward Network .....	16
3.5.1.1 Backpropagation Algorithm.....	17
3.5.2 Radial Basis Function Neural Network .....	18
3.5.3 Recurrent Networks .....	19
3.5.3.1 Elman Recurrent Algorithm.....	20
<b>CHAPTER FOUR - SYSTEM DESIGN.....</b>	<b>21</b>
4.1 Data Acquisition System .....	21
4.1.1 Microcontroller .....	21
4.1.2 Sensors .....	22
4.1.2.1 Force Sensor.....	22
4.1.2.2 Magnetic Rotary Encoder .....	25
4.1.3 Bluetooth.....	26
4.2 Hardware Implementation .....	27
4.3 Software Implementation .....	29
4.3.1 PC Application.....	29
4.3.2 Microcontroller Application .....	30
<b>CHAPTER FIVE - SIMULATION RESULTS.....</b>	<b>33</b>
5.1 Introduction .....	33
5.2 Data Normalization .....	33
5.3 Gait Patterns .....	34
5.3.1 Walking Pattern 1 .....	34
5.3.2 Walking Pattern 2 .....	38
5.3.3 Walking Pattern 3 .....	42
5.3.4 Walking Pattern 4 .....	44
5.3.5 Walking Pattern 5 .....	46
5.3.6 Walking Pattern 6 .....	48
5.4 Neural Network Applications.....	50

5.4.1 Prediction of Joint Angles .....	50
5.4.2 Detection of Gait Pattern Types .....	58
<b>CHAPTER SIX – CONCLUSIONS AND FUTURE WORK.....</b>	<b>61</b>
<b>REFERENCES.....</b>	<b>64</b>

## LIST OF FIGURES

	<b>Page</b>
Figure 2.1 Stride length and step length.....	4
Figure 2.2 Gait cycle and phases .....	6
Figure 3.1 Structure of a neural cell in the human brain.....	11
Figure 3.2 Basic elements of neuron model.....	12
Figure 3.3 Unsupervised learning rule block diagram.....	13
Figure 3.4 Supervised learning rule block diagram .....	14
Figure 3.5 Input – output curve for log-sigmoid activation function.....	15
Figure 3.6 Input – output curve for hyperbolic tangent activation function .....	15
Figure 3.7 Input – output curve for linear activation function.....	16
Figure 3.8 Structure of multilayer feedforward network .....	17
Figure 3.9 Structure of radial basis function neural network.....	19
Figure 3.10 Structure of recurrent neural network.....	20
Figure 4.1 System block ddiagram .....	21
Figure 4.2 NXP LPC1768 microcontroller board .....	22
Figure 4.3 Places of force sensitive resistor sensors on sole.....	24
Figure 4.4 Force sensitive resistor sensor .....	24
Figure 4.5 Resistance vs. force range of FSR .....	25
Figure 4.6 Magnetic rotary encoder .....	26
Figure 4.7 Bluetooth module.....	27
Figure 4.8 Overall system design with the selected microcontroller board.....	28
Figure 4.9 Schematic circuit of data acquisition system.....	28
Figure 4.10 Printed circuit board design of data acquisition system .....	29
Figure 4.11 PC application diagram .....	30
Figure 4.12 Communication protocol of encoder .....	32
Figure 5.1 Walking pattern 1 with stride length of 80 cm and step length of 40 cm, and three consecutive images from (a) to (c).....	35
Figure 5.2 Joint angles obtained from walking pattern 1 with stride length of 80 cm and step length of 40 cm (a) Left Leg (b) Right Leg (Continue).....	35
Figure 5.2 Joint angles obtained from walking pattern 1 with stride length of 80 cm and step length of 40 cm (a) Left Leg (b) Rightt Leg .....	36

Figure 5.3 Ground reaction forces obtained from walking pattern 1 with stride length of 80 cm and step length of 40 cm (a) Right Leg (b) Left Leg .....	36
Figure 5.4 Joint angles obtained from walking pattern 1 with stride length of 40 cm and step length of 20 cm (a) Left Leg (b) Right Leg .....	37
Figure 5.5 Ground reaction forces obtained from walking pattern 1 with stride length of 40 cm and step length of 20 cm (a) Right Leg (b) Left Leg .....	38
Figure 5.6 Walking pattern 2 with stride length of 80 cm and step length of 40 cm, and three consecutive images from (a) to (c) .....	39
Figure 5.7 Joint angles obtained from walking pattern 2 with stride length of 80 cm and step length of 40 cm (a) Left Leg (b) Right Leg .....	39
Figure 5.8 Ground reaction forces obtained from walking pattern 2 with stride length of 80 cm and step length of 40 cm (a) Right Leg (b) Left Leg .....	40
Figure 5.9 Joint angles obtained from walking pattern 2 with stride length of 40 cm and step length of 20 cm (a) Left Leg (b) Right Leg .....	41
Figure 5.10 Ground reaction forces obtained from walking pattern 2 with stride length of 40 cm and step length of 20 cm (a) Right Leg (b) Left Leg (Continue)....	41
Figure 5.10 Ground reaction forces obtained from walking pattern 2 with stride length of 40 cm and step length of 20 cm (a) Right Leg (b) Left Leg .....	42
Figure 5.11 Walking pattern 3 and three consecutive images from (a) to (c).....	42
Figure 5.12 Joint angles obtained from walking pattern 3 (a) Left Leg (b) Right Leg. ....	43
Figure 5.13 Ground reaction forces obtained from walking pattern 3 (a) Right Leg (b) Left Leg .....	44
Figure 5.14 Walking pattern 4 and three consecutive images from (a) to (c).....	45
Figure 5.15 Joint angles obtained from walking pattern 4 (a) Left Leg (b) Right Leg.. ....	45
Figure 5.16 Ground reaction forces obtained from walking pattern 4 (a) Right Leg (b) Left Leg .....	46
Figure 5.17 Walking pattern 5 and three consecutive images from (a) to (c).....	47
Figure 5.18 Joint angles obtained from walking pattern 5 (a) Left Leg (b) Right Leg.. ....	47

Figure 5.19 Ground reaction forces obtained from walking pattern 5 (a) Right Leg (b) Left Leg .....	48
Figure 5.20 Walking pattern 6 and three consecutive images from (a) to (c).....	49
Figure 5.21 Joint angles obtained from walking pattern 6 (a) Left Leg (b) Right Leg.. .....	49
Figure 5.22 Ground reaction forces obtained from walking pattern 6 (a) Right Leg (b) Left Leg .....	50

## LIST OF TABLES

	<b>Page</b>
Table 4.1 Specifications of NXP LPC1768 microcontroller .....	23
Table 4.2 Specifications of force sensitive resistor sensor .....	25
Table 4.3 Specifications of magnetic rotary encoder .....	26
Table 4.4 Specifications of bluetooth module.....	27
Table 5.1 Performance comparisons of LM and GDM backpropagation algorithms for walking pattern 1 with stride length of 80 cm and step length of 40 cm .....	51
Table 5.2 Performance comparisons of LM and GDM backpropagation algorithms for walking pattern 1 with stride length of 40 cm and step length of 20 cm .....	51
Table 5.3 Performance comparisons of LM and GDM backpropagation algorithms for walking pattern 2 with stride length of 80 cm and step length of 40 cm .....	51
Table 5.4 Performance comparisons of LM and GDM backpropagation algorithms for walking pattern 2 with stride length of 40 cm and step length of 20 cm .....	52
Table 5.5 Performance comparisons of LM and GDM backpropagation algorithms for walking pattern 3 .....	52
Table 5.6 Performance comparisons of LM and GDM backpropagation algorithms for walking pattern 4 .....	52
Table 5.7 Performance comparisons of LM and GDM backpropagation algorithms for walking pattern 5 .....	52
Table 5.8 Performance comparisons of LM and GDM backpropagation algorithms for walking pattern 6 .....	52
Table 5.9 Performance comparisons of neural networks depending on input data set for walking pattern 1 with stride length of 80 cm and step length of 40 cm .....	53
Table 5.10 Performance comparisons of neural networks depending on input data set for walking pattern 1 with stride length of 40 cm and step length of 20 cm .....	53
Table 5.11 Performance comparisons of neural networks depending on input data set for walking pattern 2 with stride length of 80 cm and step length of 40 cm .....	53
Table 5.12 Performance comparisons of neural networks depending on input data set for walking pattern 2 with stride length of 40 cm and step length of 20 cm .....	53
Table 5.13 Performance comparisons of neural networks depending on input data set for walking pattern 3 .....	53

Table 5.14 Performance comparisons of neural networks depending on input data set for walking pattern 4 .....	53
Table 5.15 Performance comparisons of neural networks depending on input data set for walking pattern 4 .....	54
Table 5.16 Performance comparisons of neural networks depending on input data set for walking pattern 4 .....	54
Table 5.17 Performance comparisons of multilayer perceptrons, radial basis function and Elman recurrent neural networks for walking pattern 1 with stride length of 80 cm and step length of 40 cm .....	54
Table 5.18 Performance comparisons of multilayer perceptrons, radial basis function and Elman recurrent neural networks for walking pattern 1 with stride length of 40 cm and step length of 20 cm .....	54
Table 5.19 Performance comparisons of multilayer perceptrons, radial basis function and Elman recurrent neural networks for walking pattern 2 with stride length of 40 cm and step length of 20 cm .....	55
Table 5.20 Performance comparisons of multilayer perceptrons, radial basis function and Elman recurrent neural networks for walking pattern 2 with stride length of 80 cm and step length of 40 cm .....	55
Table 5.21 Performance comparisons of multilayer perceptrons, radial basis function and Elman recurrent neural networks for walking pattern 3.....	55
Table 5.22 Performance comparisons of multilayer perceptrons, radial basis function and Elman recurrent neural networks for walking pattern 4.....	55
Table 5.23 Performance comparisons of multilayer perceptrons, radial basis function and Elman recurrent neural networks for walking pattern 5.....	55
Table 5.24 Performance comparisons of multilayer perceptrons, radial basis function and Elman recurrent neural networks for walking pattern 6.....	55
Table 5.25 Performance comparisons of neural networks depend on number of gait cycles used in training for walking pattern 1 with stride length of 80 cm and step length of 40 cm.....	56
Table 5.26 Performance comparisons of neural networks depend on number of gait cycles used in training for walking pattern 1 with stride length of 40 cm and step length of 20 cm.....	56

Table 5.27 Performance comparisons of neural networks depend on number of gait cycles used in training for walking pattern 2 with stride length of 80 cm and step length of 40 cm.....	56
Table 5.28 Performance comparisons of neural networks depend on number of gait cycles used in training for walking pattern 2 with stride length of 40 cm and step length of 20 cm.....	57
Table 5.29 Performance comparisons of neural networks depend on number of gait cycles used in training for walking pattern 3 .....	57
Table 5.30 Performance comparisons of neural networks depend on number of gait cycles used in training for walking pattern 4 .....	57
Table 5.31 Performance comparisons of neural networks depend on number of gait cycles used in training for walking pattern 5 .....	57
Table 5.32 Performance comparisons of neural networks depend on number of gait cycles used in training for walking pattern 6 .....	57
Table 5.33 Training performance comparisons depending on the number of neurons in the hidden layer and angle input data set .....	58
Table 5.34 Success rate of LVQ NN for test data sets consist from joint angles .....	58
Table 5.35 Training performance comparisons depending on the number of neurons and combination of input data sets in the hidden layer .....	59
Table 5.36 Success rate of LVQ NN for test data sets consist from combination of input data sets.....	59
Table 5.37 Success rate of MLP NN for detection of four types of gait patterns.....	60
Table 5.38 Success rate of MLP NN for detection of two types of gait patterns.....	60
Table 5.39 Success rate of LVQ NN for detection of two types of gait patterns.....	60

# CHAPTER ONE

## INTRODUCTION

### 1.1 Introduction

Gait analysis is a type of study which examine walking motion depending on mathematical analyses. This analysis contains measurement, description and assessment of quantities that characterize human motion. To determination of gait cycles, calculation of walking speed and detection of gait disturbances can be a few examples obtained on gait analysis. Gait analysis is applied for interdisciplinary studies (Toygar, et al., 2012; Capi, Nasu, Barolli, & Mitobe, 2002; Betker, Maharjan, Yaduvanshi, Szturm, & Moussavi, 2008).

Gait analysis studies can be used for health diagnostics and rehabilitation exercise (Baker, 2006; Kwon & Gross, 2005; Wahab & Bakar, 2011). For instance; detection of gait disturbances and observation of healing period for patients can be observed. But, gait analysis systems are very expensive and need to have well environmental conditions in laboratory.

Nowadays, wearable sensors are more popular for gait analysis depending on cheaper and portability (Sant'Anna, Wickström, Eklund, & Tranberg, 2012; Bamberg, Benbasat, Scarborough, Krebs, & Paradiso, 2008; Pulliam, Lambrecht, & Kirsch, 2011; Whittle, 2007; Tao, Liu, Zheng, & Feng, 2012). Wearable sensors mean that they can be mounted on various parts of human's body like joints and sole. These sensors may be accelerometers, encoders, goniometers, gyroscopes, EMG, force sensors. The movement signals can be recorded by these sensors and they can be used to perform the gait analysis. For example; angle of joints (knee, hip and ankle), electrical signals of muscles, velocity of walking, and ground reaction forces along walking can be calculated easily.

In the literature, there are numerous studies depending on gait analysis (Pawin, Khaorapapong, & Chawalit, 2011; Kutilek & Farkasova, 2011; Pinitlertsakun &

Charoensuk, 2012; Kong & Tomizuka, 2008; Barton & Lee, 1995; Wang & Buchanan, 2002; Pappas, Popovic, Keller, Dietz, & Morari, 2001). These are determination of gait cycles and phases, detection of gait abnormalities, classification of gait patterns, kinetic and kinematic analysis along the walking, and prediction of joint angles in particular. In the thesis, studies are applied for detection of gait patterns and prediction of joint angles by using neural networks.

## **1.2 Thesis Outline**

Chapter 1 presents an introduction to the project.

Chapter 2 presents general knowledge on gait analysis, including gait parameters, gait cycle and phases. It also introduces popular sensors used for data gathering.

Chapter 3 gives some theoretical information about basics of artificial neural networks and explains artificial neural network architectures and algorithms like multilayer perceptron, radial basis function and recurrent neural network.

In Chapter 4, design of data acquisition system used to collect gait data is described. Hardware, software and sensors used in data acquisition system gives information.

In Chapter 5, gait patterns and obtained data by using data acquisition system are introduced. Comparisons are given about performances of studies realized with artificial neural networks. Moreover, neural networks are used to recognize patterns of human movement.

In Chapter 6, conclusion and future works are presented.

## **CHAPTER TWO**

### **GAIT ANALYSIS**

#### **2.1 Introduction**

Human gait analysis is the systematic study of human walking that has been developed from early illustrative studies to modern studies involving mathematical analysis and modelling. It has become a significant part of human motion analysis. This type of analysis involves measurement, description, and assessment of quantities that characterize human walking. For instance, through gait analysis, the gait phase can be identified, the kinematic and kinetic parameters of human gait events can be determined, and musculoskeletal functions can be quantitatively evaluated. Gait analysis has been applied in numerous areas like biomechanical, psychological, and security disciplines (Tao, Zheng, Liu, & Feng, 2012).

Gait analysis studies can be used for sports, rehabilitation, and health diagnostics. But, gait analysis facilities are limited. For example; to recognize the faults in player performances, to monitor patient's healing period and to distinguish between healthy people and patients with medial knee osteoarthritis based on accelerometers was investigated. Existing many gait analysis systems are expensive and need good environment conditions such as laboratory. Nowadays, wearable sensors are very popular to have gait analysis (Gabel, Gilad-Bachrach, Renshaw, & Schuster, 2012).

In gait analysis, sensors are attached to various parts of the human's body like foot, knee, ankle and hip. These sensors, which may be accelerometers, gyro sensors, force sensors, encoders, goniometers, and so on, can measure various characteristics of the human gait. The movement signal recorded by these sensors can be used to perform the gait analysis.

## 2.2 Gait Parameters

The general gait parameters are stride length, cadence and speed. These parameters can give about information on gait characteristics of a subject. These values can change according to subject's age and sex.

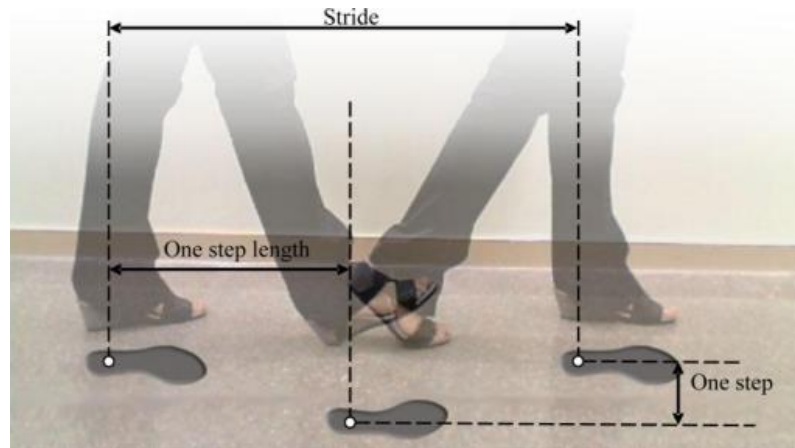


Figure 2.1 Stride length and step length (Teixido, Palleja, Tresanchez, Nogues, & Palacin, 2011)

Stride length shown in figure 2.1 is measured with distance between same two contacts of the same foot. If speed and gait cycle time can be known, stride length can be calculated with equation 2.1 (Whittle, 2007).

$$\text{Stride length (m)} = \text{Speed (m/s)} \times \text{Cycle time (s)} \quad (2.1)$$

One stride length have two step lengths.

Cadence is the number of steps per minute. It can be measured with aid of a stopwatch and by counting the number of steps realized during a known period of time as seen in equation 2.2 (Whittle, 2007).

$$\text{Cadence (steps/min)} = \text{Counted Steps} \times 60/\text{Time (s)} \quad (2.2)$$

The number '60' in the formula shows 60 seconds in a minute.

Speed is measured from the time taken to walk a known distance and by watching carefully the number of steps taken in that time can be counted. The formula is given in equation 2.3 (Whittle, 2007).

$$\text{Speed (m/s)} = \text{Distance (m)}/\text{Time (s)} \quad (2.3)$$

Although every person has self-selected walking speed, the actual speed is continuously adjusted according to the conditions. Speed can be slowed or increased to avoid accidents with vehicles, and is consciously varied according to different situations (Kirtley, 2006).

Stride length, cadence and speed are also called the temporal-spatial parameters of gait, and they create the basis of any gait assessment (Kirtley, 2006).

### **2.3 Gait Cycle**

Gait cycle consists of from one foot touch the ground to the time the same part of same foot touch ground again. Gait cycle can be divided into phases. Each gait cycle has main sub-phases. These are stance phase and the swing phase. Stance and swing phases compose approximately 62% and 38% of the gait cycle in a normal gait pattern. The stance phase is the portion of the gait cycle when the foot is in contact with the ground. It is initiated by heel strike and ends with toe off of the same foot. Swing phase is the portion of the gait cycle when the foot is in air. It is initiated with toe off and ends with heel strike. Stance and swing periods can further be divided into subgroups (Perry, 1992).

#### **2.3.1 Gait Phases**

Different terminologies are used to describe phases of gait cycle. These are traditional terminology and Rancho Los Amigos (RLA) system (Dreeben-Irimia, 2011; Lippert, 2011). The traditional terminology developed for gait rehabilitation mounted after World War II to improve lower extremity prosthetics. It describes gait in terms of heel strike, foot flat, midstance, heel off, toe off, acceleration, midswing and deceleration. The Rancho Los Amigos (RLA) terminology became more and more popular in the late 1980's and early 1990's and is currently used as standard among clinicians. It describes gait more in terms of processes or segments of time, such as initial contact, loading response, midstance, terminal stance, pre-swing,

initial swing, midswing and terminal swing. It is more general and better enclose the common features of normal and pathological gait.

### 2.3.1.1 Rancho Los Amigos Terminology

This terminology consist of eight phases (Cuccurullo, 2010; Lippert, 2011; Dreeben-Irimia, 2011). These are initial contact, loading response, midstance, terminal stance, preswing, initial swing, midswing and terminal swing. Terminology is shown in the Figure 2.2.

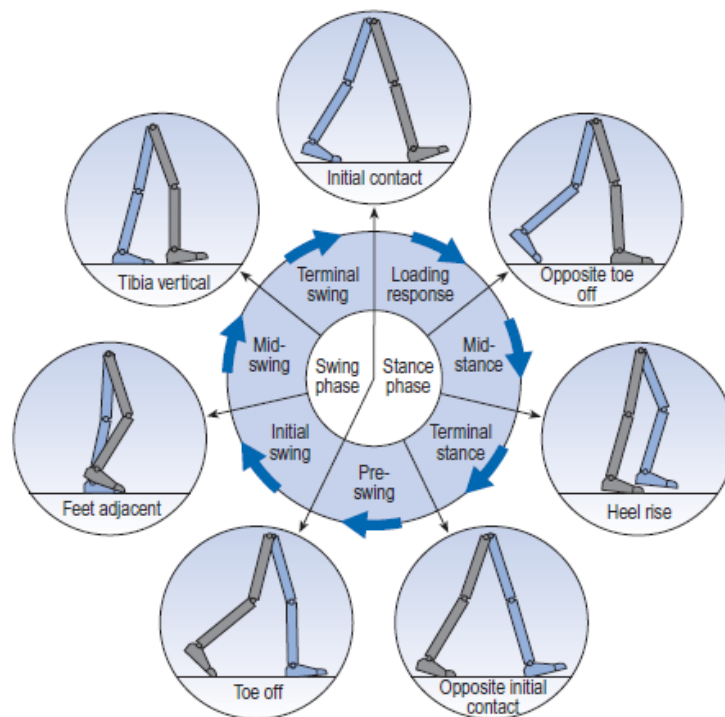


Figure 2.2 Gait cycle and phases (Whittle, 2007)

Initial Contact is only an instantaneous point in time and occurs the instant the foot of the leading lower limb touches the ground. It represents the beginning of the stance phase.

Loading Response begins with initial contact and continues until the other foot is lifted for swing. During loading response, the foot comes in full contact with the floor, and body weight is fully transferred onto the stance limb. Its interval is between 0-10% of gait cycle.

Midstance begins when the contralateral foot leaves the ground and continues as the body weight travels along the length of the foot until it is aligned over the forefoot. The initial peak of the force graph shows the period of mid-stance. Its interval is between 10-30% of gait cycle.

Terminal stance begins with heel rise and ends when the contralateral foot contacts the ground. During this phase, body weight moves ahead of the forefoot. Its interval is between 30-50% of gait cycle.

Preswing begins when the contralateral foot contacts the ground and ends with ipsilateral toe off and body weight is transferred onto the contralateral limb. Its interval is between 50-62% of gait cycle.

Initial Swing is the first third of the swing phase. It begins the moment the foot leaves the ground and continues until maximum knee flexion occurs. Its interval is between 62-75% of gait cycle.

Midswing is the middle third of the swing phase. It begins when the swinging foot is opposite the stance foot and ends when the swinging limb is forward. Its interval is between 75-85% of gait cycle.

Terminal Swing is final phase of gait cycle. It begins with vertical tibia and ends when the foot strikes the floor. Its interval is between 85-100% of gait cycle.

## **2.4 Sensors for Gait Analysis**

Different sensors are used on various parts of the human's body like foot, knee, ankle and hip for gait analysis. Sensors like accelerometers, gyro sensors, force sensors, encoders, and goniometers in particular, are very popular various

characteristics of the human gait in nowadays. The movement signal recorded by these sensors can be used to perform the gait analysis.

Force Sensor can be embedded to have ground reaction forces particular area in the foot along walking. Many different types of force sensor have been used practically, containing resistive and capacitive strain gauges, conductive rubber, piezoelectric materials and a photoelastic optical system (Whittle, 2007).

Goniometer is connected to the lower extremity for making measurements of the angle of a joint, including hip, knee and wrist. The output of goniometer is usually plotted as joint angle against time. At the same time, if measurements have been made from two joints like hip and knee, the data can be plotted as an angle-angle diagram, also known as a 'cyclogram'. This format shows that the interaction between the two joints and makes it possible to recognize patterns (Djuric-Jovicic, Jovicic, & Popovic, 2011).

Accelerometer is a type of inertial sensor that can measure acceleration along its sensitive axis. By attaching these accelerometers to the feet or legs, the acceleration/velocity of the feet or legs in the gait can be determined to perform the gait analysis. Three common types of accelerometers are available, namely, piezoelectric, piezoresistive, and capacitive accelerometers. Piezoresistive and capacitive accelerometers can provide dual acceleration components and have higher stability (Tao, Zheng, Liu, & Feng, 2012).

Gyroscope can be used to measure the orientation of the body segments in space and to measure angular velocity and acceleration. Angular velocity and angle of feet or legs during the gait can identify the rearrangement of the various gait phases by attaching a gyroscope to human feet or legs. It is always combined with an accelerometer to build a perfect initial sensing system (Tao, Zheng, Liu, & Feng, 2012; Whittle, 2007).

Electromyography is used to measure the electrical activity of the muscles in the lower extremity along walking. The three methods of recording the EMG are by way of surface, fine wire and needle electrodes. Generally, surface electrodes are used when general information on muscle activity is required. Wire electrodes must be inserted into muscle using a needle to have specific information on a muscle. Accordingly, EMG sensors can be used to realize the assessment of muscle activity in human gait and play an important role in evaluating the walking performance of individuals with problems in their lower extremities (Tao, Zheng, Liu, & Feng, 2012).

## **2.5 Gait Analysis Methods**

Kinematic analysis is the measurement of movement, which is the geometric description of motion, in terms of displacements, velocities and accelerations. Kinematic systems are used to record the position and orientation of the body segments for gait analysis, the angles of the joints and the corresponding linear and angular velocities and accelerations. Based on these gait data, a kinematic analysis can be performed to recognize the gait phases, as well as obtain the general gait parameters and movement information on the body segments (Tao, Zheng, Liu, & Feng, 2012).

Kinetic analysis is used to calculate the net forces and moment make effort on the body due to the combination of the ground reaction force, inertia, and muscle contraction. Kinetic analysis requires the collection of kinematic information and ground reaction forces at the same time. Ground reaction forces are collected from people walk on force plates placed into the floor. The calculation of forces and moments produce at each joint is based on inverse dynamic method (Vaughan, Davis, & O'Connor, 1999).

Electromyography is used to determine electrical activation of muscles and to calculate the relative magnitude of muscle contraction. EMG data can be collected with electrodes, including surface, needed, or intramuscular wire electrodes. The

EMG signal is amplified and transmitted via cable or wireless to a computer where it is synchronized with kinematic and kinetic data. It also allows the inference about motion abnormalities (Whittle, 2007).

## CHAPTER THREE

### ARTIFICIAL NEURAL NETWORKS

Artificial neural network is mathematical model of central nervous system. Many disciplines use it to solve different problems like pattern recognition, prediction, optimization and control.

#### 3.1 The Biological Model

The human brain consists of more than billions of neural cells that process information. Each cell works like a simple processor. Brain's ability is provided with communication between cells and their parallel processing.

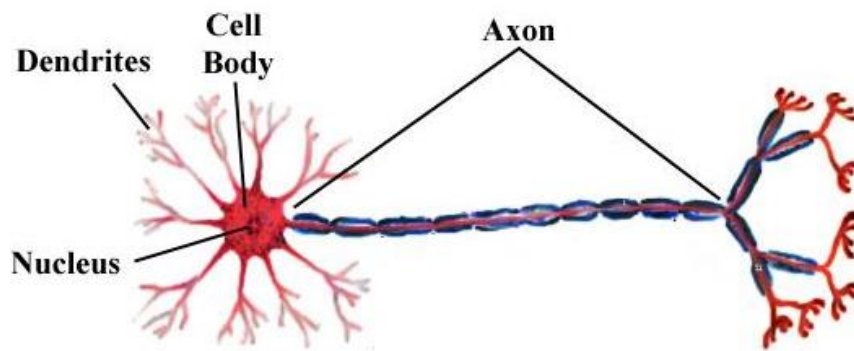


Figure 3.1 Structure of a neural cell in the human brain (Fröclich, 1996)

As shown in the Figure 3.1, a neuron consists of a nucleus, dendrites and an axon. Information between neurons is transferred with electrical stimulations together on dendrites. Incoming information that arrive the neuron's dendrites is summed up and then delivered along the neuron's axon. The information is passed to other neurons when the stimulation has exceeded specific threshold. In this case, the neuron is activated. If the incoming stimulation is too low that is it hasn't got enough threshold value, the information won't be transported. In this case, the neuron is told to be inhibited. The connection structure between the neurons changes dynamically. It is accepted that the learning ability of the human brain is based on this structure (Fröclich, 1996).

### 3.2 Basic Elements of Artificial Neuron Model

An artificial neuron is a mathematical function conceived as a simple model of a real neuron. The early model of an artificial neuron is introduced by Warren McCulloch and Walter Pitts in 1943. This is also simplified model of a real neuron (Rojas, 1996). The neuron consist of three basic components, including weight factors, thresholds, and activation function as shown in figure 3.2.

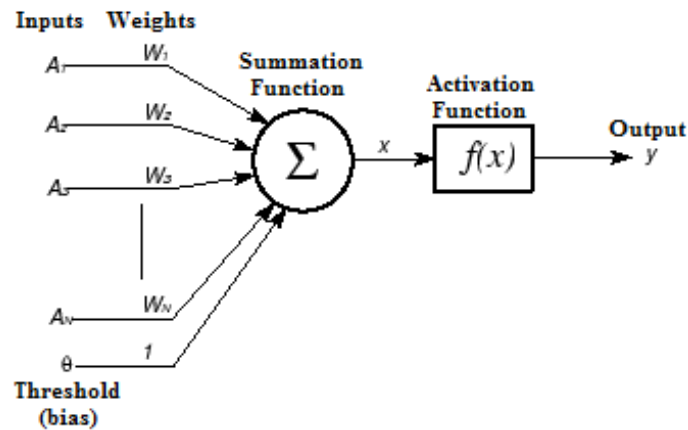


Figure 3.2 Basic elements of neuron model (Touzed, n.d.)

In figure 3.2, let's consider input vector as  $A=[A_1, A_2, A_3, \dots, A_N]$ . Each input is multiplied by the related weight of the neuron connection ( $I=A^T * W$ ).  $W=[W_1, W_2, W_3, \dots, W_N]$  are weight values normalized in the range of either (0,1) or (-1,1).

The threshold allows to shift the activation function to the left or right, which may be critical for successful learning. The threshold in artificial neuron is usually represented by  $\theta$ . It can be negative or positive. If it is positive, it is referred as bias. If threshold input is '1' and its weight  $W_0 = \theta$  are assumed, formula will be given in equation 3.1.

$$y=f(A^T W+\theta) \tag{3.1}$$

Activation functions perform a mathematical operation on the signal output for better solution. They have different types. The most popular of them are sigmoid, tangent hyperbolic and linear functions.

### 3.3 Learning Rules in Neural Networks

There are three types of neural network learning rules (Hagan, Demuth, & Beale, 1996; Haykin, 2005). Unsupervised and supervised learning rules are particularly used to train the network.

In unsupervised learning rule given in figure 3.3, training set consist of only input training data. There are no target outputs available. The network learns to adapt based on the experiences collected through the previous training patterns.

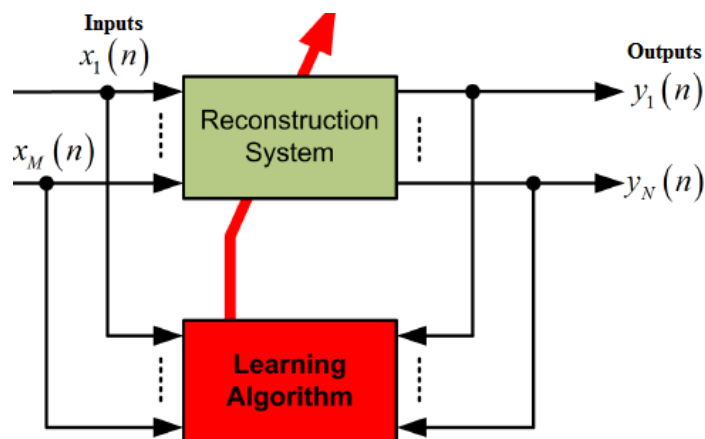


Figure 3.3 Unsupervised learning rule block diagram (Chakraborty, 2007)

In supervised learning rule shown in figure 3.4, training set consist of both input and output training patterns. Targets are known and given in input to the model during the learning process. The learning rule is then used to adjust the weights and biases of the network in order to move the network outputs closer to the targets.

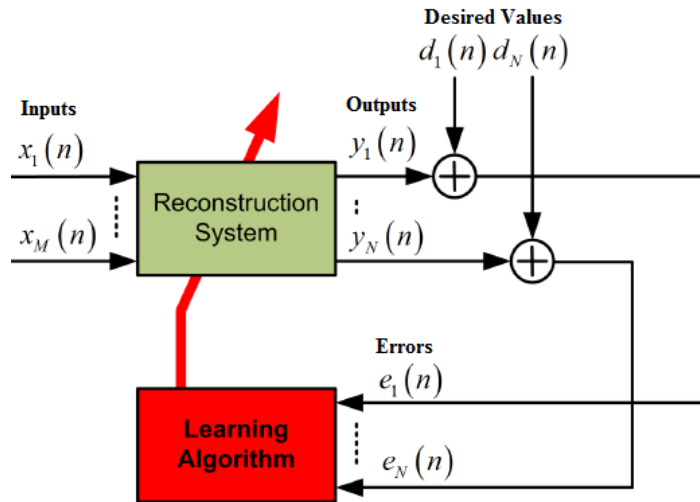


Figure 3.4 Supervised learning rule block diagram (Chakraborty, 2007)

### 3.4 Types of Activation Functions

ANN transfer functions are used to simulate reaction of system using input and out parameters. A variety of transfer function have been included in literature (Hagan, Demuth, & Beale, 1996; Dorofki, Elshafie, Jaafar, Karim, & Mastura, 2012).

These can be linear or nonlinear functions. Transfer functions provides simulation that visualizes the input-output behavior of an artificial neuron depending on the specific combination of linear and nonlinear transfer functions three of these functions are the most commonly used. These are linear, log-sigmoid and hyperbolic tangent sigmoid transfer functions.

#### 3.4.1 Log-Sigmoid Activation Function

Input values changes between  $-\infty$  and  $+\infty$ , however, the output values are in the range of 0 and 1. The mathematical formula for this function is shown in equation 3.2 (Hagan, Demuth, & Beale, 1996).

$$a = \frac{1}{1 + e^{-n}} \quad (3.2)$$

The log-sigmoid transfer function given in figure 3.5 is a nonlinear function and it is used in multilayer networks that are used for training of the backpropagation algorithm in particular since this transfer function is differentiable.

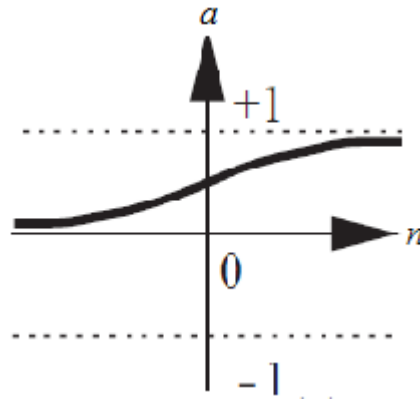


Figure 3.5 Input – output curve for log-sigmoid activation function (Dorofki, et al., 2012)

### 3.4.2 Hyperbolic Tangent Sigmoid Activation Function

This transfer function is similar to the sigmoid transfer function. Difference from sigmoid transfer function is that hyperbolic tangent sigmoid function has a range from -1 to 1. Since it has large range, the hyperbolic activation function is commonly used instead of sigmoid transfer function. The input and output curve of the hyperbolic tangent function can be seen in Figure 3.6.

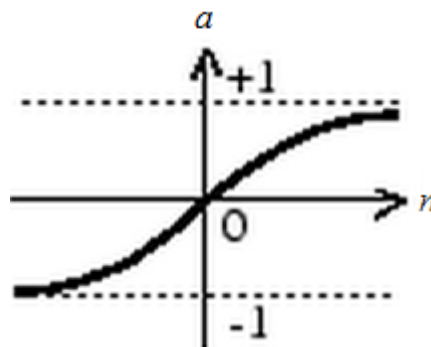


Figure 3.6 Input – output curve for hyperbolic tangent activation function (Dorofki, et al., 2012)

The mathematical formula for the hyperbolic tangent activation function is shown in equation 3.3 (Hagan, Demuth, & Beale, 1996).

$$a = \frac{e^n - e^{-n}}{e^n + e^{-n}} \quad (3.3)$$

### 3.4.3 Linear Activation Function

The output is equal to its input at linear transfer function. The mathematical formula for linear transfer function is shown in equation 3.4 (Hagan, Demuth, & Beale, 1996).

$$a=n \quad (3.4)$$

The input and output curve of the hyperbolic tangent function can be seen in figure 3.7.

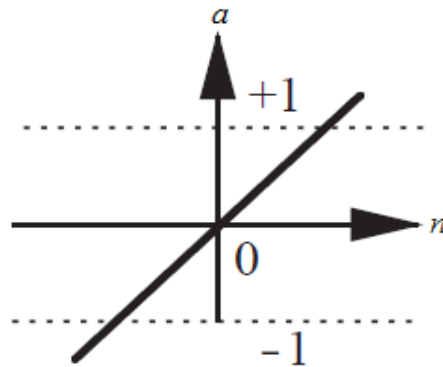


Figure 3.7 Input – output curve for linear activation function (Dorofki, et al., 2012)

## 3.5 Network Architectures

Commonly one neuron, even with many inputs, may not be sufficient. Sometimes, we need more neurons operate in parallel. These neuron community is called as a layer. According to number of layer and working type of neurons, network architectures are created. These are single layer feedforward, multilayer feedforward and recurrent networks (Hagan, Demuth, & Beale, 1996; Haykin, 2005).

### 3.5.1 Multilayer Feedforward Network

This kind of feedforward network has one or more hidden layers in addition to input and output layers. The computational units of the hidden layer are known as hidden neurons. Block diagram is shown in figure 3.8.

Multilayer networks has more advantages than single layer networks. For instance, two layer networks can be trained with both a sigmoid in first layer and a linear function in second layer for better results.

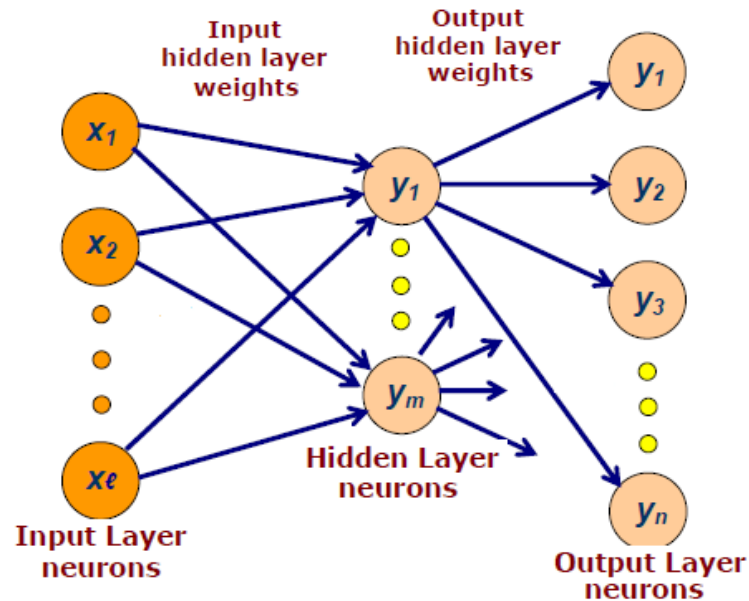


Figure 3.8 Structure of multilayer feedforward network (Chakraborty, 2007)

One of the most important problems is which one can predict the optimal number of neurons in a hidden layer. There is no clear definition for this. But, most practical neural networks have two or three layers. Four or more layers are used seldom (Galushkin, 2007).

### 3.5.1.1 Backpropagation Algorithm

Backpropagation networks are probably the most popular algorithm applied on neural networks. It is a form of supervised learning for multilayer networks. It has an input layer, hidden layers and output layer.

During the training of the network, inputs and targets are presented. The input causes output responses in each layer and an output consist at the output layer. At the output layer, the difference between the actual output and target provides an error. This error depends on the values of the weights of the neurons in each layer. This

error is minimized, and during this process new values for the weights are obtained. The speed and accuracy of the learning process are provided with learning rate.

At the beginning of backpropagation network training, we have to get input and target values, learning rate coefficient, criterion that terminates the algorithm, methodology for updating weights, nonlinear or linear function and initial values for weight and bias. Nonlinear function can be sigmoid or tangent function. Initial values should choose small random values. There are different train algorithms for backpropagation network. The most popular are gradient descent momentum algorithm and Levenberg-Marquardt (Hagan, Demuth, & Beale, 1996).

### ***3.5.2 Radial Basis Function Neural Network***

Radial basis networks may require more neurons than feedforward back propagation networks (Haykin, 2005). They can work best when many training vectors are available. A common learning algorithm for RBF is based on first choosing randomly some data points as radial basis function centers.

RBF network consists of two layers, including a hidden radial basis layer and an output linear layer of neurons. Different types of RBF network could be used, but the most common is Gauss Function. Network architecture is shown in figure 3.9.

A RBF network can be regarded as a special two layer network which is linear in the parameters by fixing all RBF centers and nonlinearities in the hidden layer. Thus, hidden layer performs a fixed nonlinear transformation with no adjustable parameters and it maps the input space onto a new space. The output layer then implements a linear combiner on this new space, and only adjustable parameters are weights of this linear combiner. Because of strong connection between RBF and neural networks, it is reasonable to believe that an RBF network can offer approximation capabilities similar to those of the two layer neural network, provided that the hidden layer of the RBF network is fixed appropriately (Haykin, 2005).

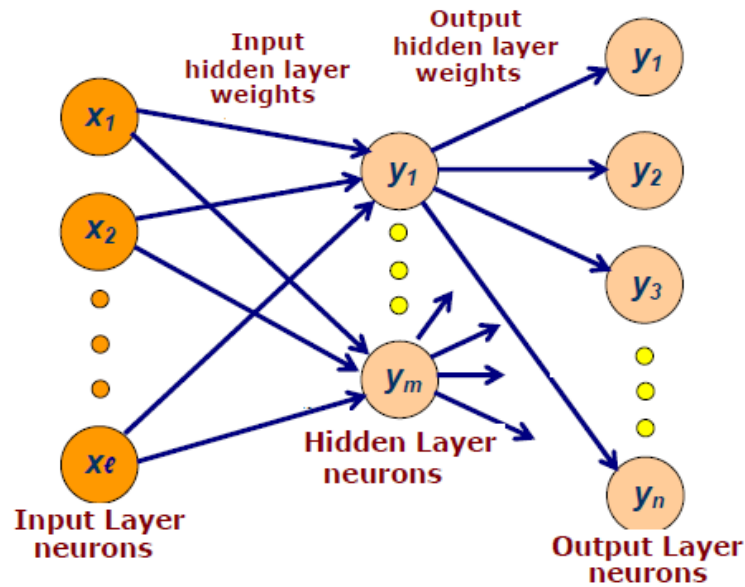


Figure 3.9 Structure of radial basis function neural network (Chakraborty, 2007)

Performance of RBF network depends on the chosen centers. In practice, the centers can be chosen to be a subset of the data. Center or radius are also called as “spread”. With larger spread, neurons at a distance from a point have a greater influence. With small spread, they are very selective.

### 3.5.3 Recurrent Networks

Recurrent networks differ from feed-forward architecture since it has at least one feedback loop (Mandic & Chambers, 2001). Neurons can make feedback themselves or other neurons. Block diagram of recurrent network is shown in figure 3.10.

Recurrent networks are more powerful than feedforward networks since it can exhibit temporal behavior.

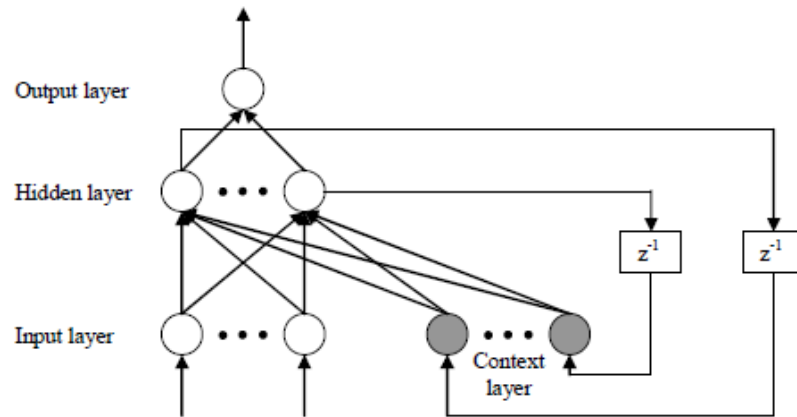


Figure 3.10 Structure of recurrent neural network

### 3.5.3.1 Elman Recurrent Algorithm

The Elman network is a type of recurrent network. This type of network has input layer, hidden layer, context layer and output layer. The inputs and output values consist of outside environment and these values don't change. Output layer is a linear unit. Hidden layers can be linear or nonlinear transfer functions. Context layer is a memory to hold previous events of the hidden layers. It is also a function that is used as time delay. Recurrent connections that is between hidden layer and context layer are fixed. In literature, it is sometimes called as partially recurrent network because of fixity. Elman network architecture is given in figure 3.10 (Pham, & Liu, 1996).

All connections between neurons are indicated with a weight like multilayer feedforward neural network architecture. Firstly, weight values are selected as small values and are optimized during training. The weights between the hidden layers and context layer are set to one and are fixed. The values of the context neurons are transferred precisely. Initial output weights of the context neurons are equal to half the output range of the other neurons in the network. The Elman network can be trained with gradient descent backpropagation or Levenberg-Marquardt algorithm. The backpropagation algorithm causes some problems for some applications. Because, the algorithm doesn't provide to find the global minimum of the error function. Cause of this is that gradient descent training algorithm may have troubles to find local minima (Haykin, 2005).

## CHAPTER FOUR SYSTEM DESIGN

### 4.1 Data Acquisition System

The data acquisition system used to collect data is a wearable system consisting of five parts, including sensors, microcontroller, bluetooth module, battery and personal computer (PC). The sensors and bluetooth module make communication with microcontroller on digital and analog interfaces. The microcontroller transfers the obtained data to PC via bluetooth module. A block diagram of the system is shown in figure 4.1.

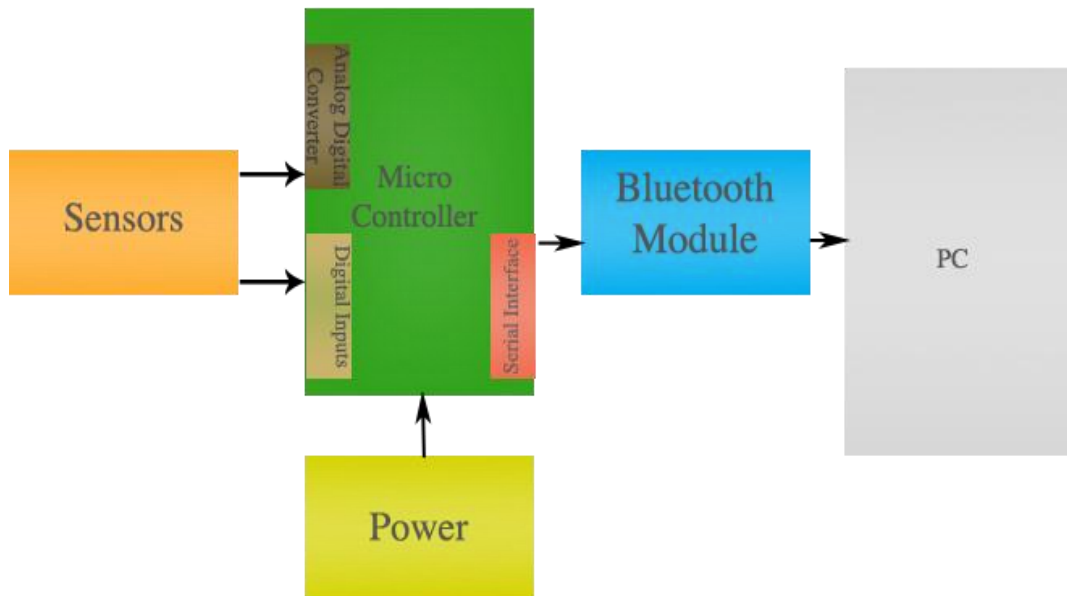


Figure 4.1 System block diagram

#### 4.1.1 Microcontroller

MBED NXP LPC1768 microcontroller board has been chosen as platform due to some of its useful features for study. One of the most important features is to consume ultra-low power. This microcontroller is very suitable for mobile measurement due to its size, computation ability and speed applications. On chip analog digital converter has 8 channel and 12-bit resolution with internal precision

reference. The microcontroller can sample at up to 200 KHz samples/sec. This is a sufficiently high sampling rate that the device can be used to measure even more strenuous activities, such as walking. Another advantage is that board has flash memory, which can support up to 512Kbyte. With this function it was possible to create a data logger and record data during short time intervals such as one minute. The board has some other desirable features such as a free programming environment. It can be also programmed via USB OTG connector. It has two regulators that gives 3.3V and 5V (NXP, 2009). MBED LPC 1768 board is shown in figure 4.2.

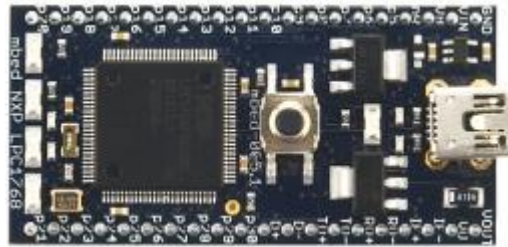


Figure 4.2 NXP LPC1768 microcontroller board

The features of the LPC1768 board are shown in Table 4.1 (NXP, 2009)

#### **4.1.2 Sensors**

##### *4.1.2.1 Force Sensor*

Six force sensors (three for each foot) has been placed into the sole of shoes. In Rana's research, foot pressure distribution is examined to find ideal position of force sensors (Rana, 2009). Healthy people were used to determine sensor zones under foot and eight zones were identified for his aim. Force sensors are to be placed as illustrated in figure 4.3.

Table 4.1 Specifications of NXP LPC1768 microcontroller

LPC1768	
Arm Cortex M3 Core	<ul style="list-style-type: none"> <li>• 100 MHz operation</li> <li>• Memory protection unit</li> <li>• Four power mode: sleep, deep sleep, power down, and deep power down</li> </ul>
Memories	<ul style="list-style-type: none"> <li>• 512 KB of flash memory</li> <li>• 64 KB of SRAM</li> </ul>
Serial Peripherals	<ul style="list-style-type: none"> <li>• 10/100 Ethernet MAC</li> <li>• USB 2.0 full-speed device/Host/OTG controller with on-chip PHY</li> <li>• Four UARTs with fractional baud rate generation</li> <li>• Two CAN 2.0B controllers</li> <li>• Three SSP/SPI controllers</li> <li>• Three I2C-bus interfaces with one supporting Fast Mode Plus (1-Mbit/s data rates)</li> <li>• I2S interface for digital audio</li> </ul>
Analog Peripherals	<ul style="list-style-type: none"> <li>• 12 bit ADC with 8 channels</li> <li>• 10 bit DAC</li> </ul>
Other Peripherals	<ul style="list-style-type: none"> <li>• Ultra low power (&lt; 1<math>\mu</math>A) RTC</li> <li>• Four 32-bit general purpose timers</li> </ul>

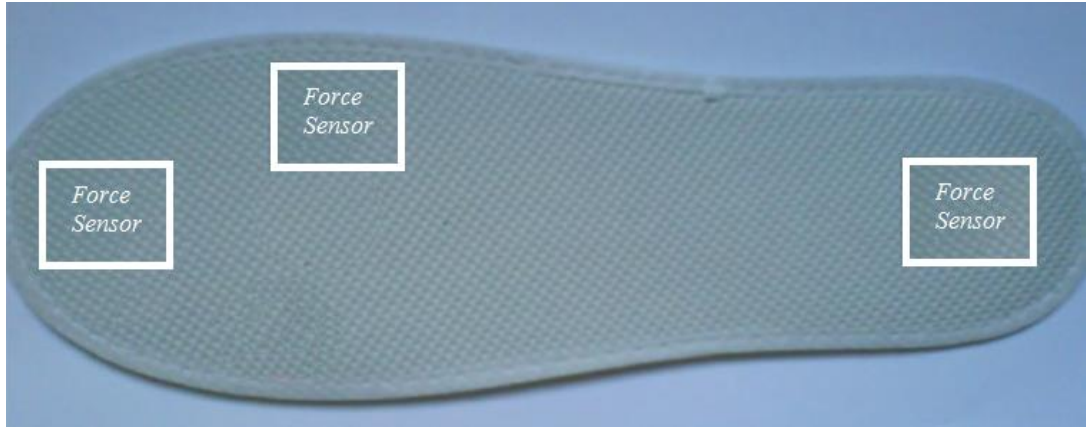


Figure 4.3 Places of force sensitive resistor sensors on sole

Various factors were considered for sensor selection. Firstly, the sensors must be very thin to provide walking comfort. Secondly, good linearity and repeatability are desired in order to obtain accurate data. Moreover, there are also some additional parameters, including maximum load, response time, etc. that must be acquired in the gait analysis.

There are many systems that can be used for experiment. But, in this study, we developed our own system to measure ground reaction forces because of limited budget. Force Sensing Resistors (FSRs) were chosen due to advantages. Figure 4.4 shows the FSR sensor and its sensing area.

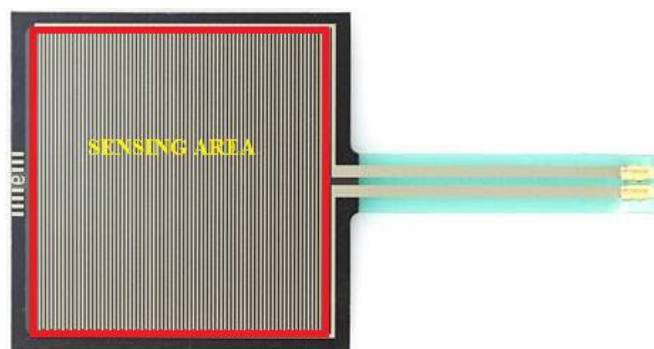


Figure 4.4 Force sensitive resistor sensor (Sparkfun, n.d.)

The specifications of the sensor is given in table 4.2 (Interlink Electronics, 2010)

Table 4.2 Specifications of force sensitive resistor sensor

Properties of FSR	
Thickness	0,45 mm
Length	88 mm
Width	43,69 mm
Sensing Area	38,1x38,1 mm
Standard Force Range	100 g – 10 kg
Hysteresis	±10%
Repeatability	±2%
Resolution	Continuous

FSR sensors are a polymer thick film device which exhibits a decrease in resistance with an increase in the force applied to the active surface. The force versus resistance characteristic shown in Figure 4.5 provides an overview of FSR typical response behavior. Break force or, turn on threshold resistance is greater than 100kΩ. The area where the force is being applied, such as the center of a large FSR device, will give it a lower resistance (Interlink Electronics,2010).

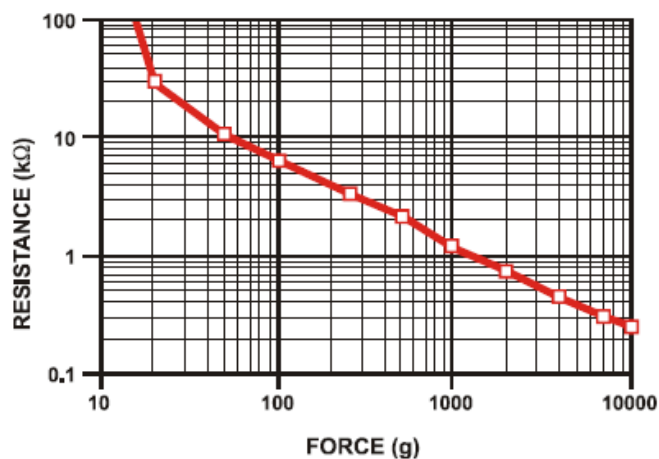


Figure 4.5 Resistance vs. force range of FSR (Interlink Electronics, 2010)

#### 4.1.2.2 Magnetic Rotary Encoder

Encoders are attached to obtain joint angles. For this purpose, Dokuz Eylul University Mechanical Engineer Department designed a mechanic system that can be

mounted on lower extremity. Sensors shown in figure 4.6 attached to knee, hip and ankle joint areas of mechanical design.



Figure 4.6 Magnetic rotary encoder (OPKON Electronics, n.d.)

The specifications of magnetic rotary encoder is shown in table 4.3 (OPKON Electronics, n.d.).

Table 4.3 Specifications of magnetic rotary encoder

Specifications of Encoder	
Resolution	10 bit
Output Signal	TTL
Supply Voltage	5V (DC)
Maximum cycle	1000 rpm
Range	Up to around 10m
Range of Working Temperature	-20 ... +80 °C
Case Diameter	50mm
Rod Diameter	8mm

#### **4.1.3 Bluetooth**

Bluetooth is used to make wireless communication with computer. Bluetooth module shown in figure 4.7 gives the flexibility to send the obtained information to PC during the walking. This certainly gives advantage for ascending and descending stairs.



Figure 4.7 Bluetooth module (Gökçegöz, 2013)

The reason to choose this module is the small size, cost and communication range. The specifications of the bluetooth module are given in table 4.4 (Core Electronics, n.d.).

Table 4.4 Specifications of bluetooth module

Specifications of Bluetooth Module	
Interface	UART
Bit Rate	Up to 3Mbps
Voltage	3.3 to 5V
Current	40 mA max
Range	Up to around 10m
Memory	External 8Mbit Flash
Baud rate	Up to 921600Kbps
Dimensions	40x18.5mm

## 4.2 Hardware Implementation

A more detailed overview of the structure of the data acquisition system is shown in figure 4.8. As can be seen from diagram, system have sensors, bluetooth module, power battery and microcontroller.

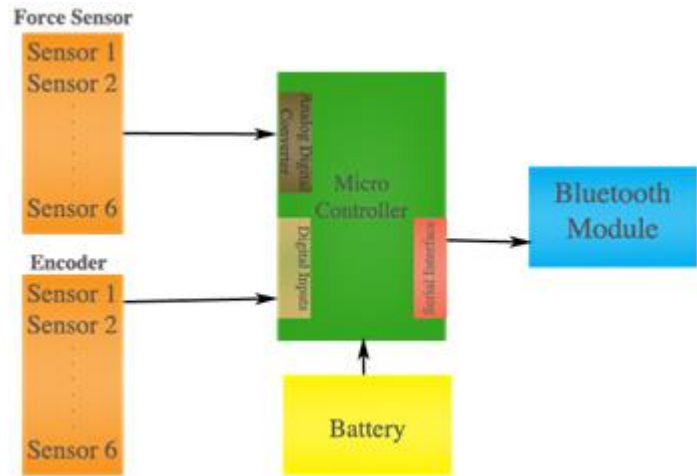


Figure 4.8 Overall system design with the selected microcontroller board

According to block diagram, schematic circuit is given in figure 4.9.

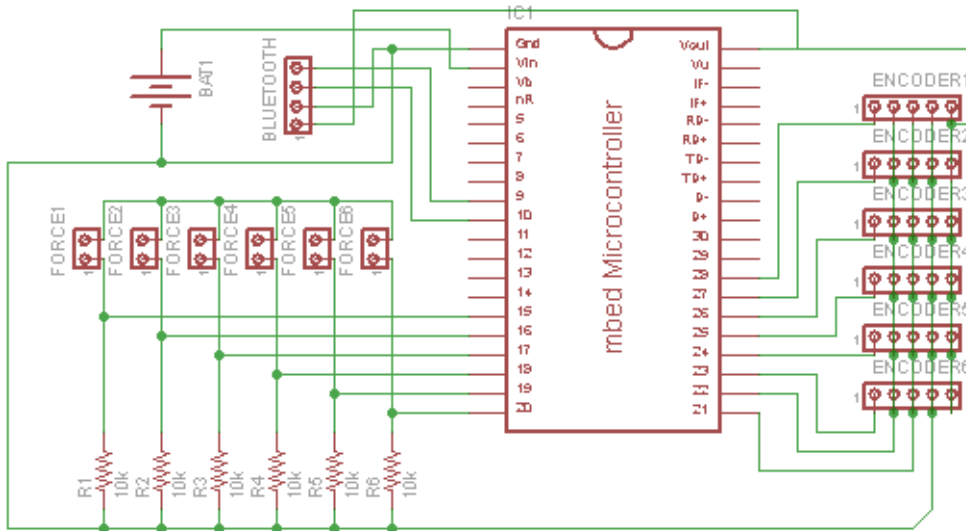


Figure 4.9 Schematic circuit of data acquisition system

Printed circuit board (PCB) design of the complete system is given in figure 4.10.

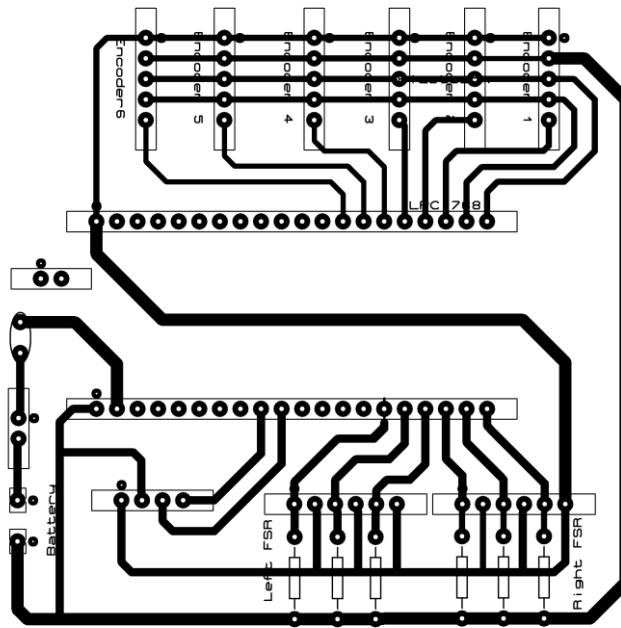


Figure 4.10 Printed circuit board design of data acquisition system

The sensors, bluetooth, and microcontroller board compose the wearable portion of the gait analysis device. This wearable system will be worn by the amputation patients or healthy people on their lower leg limb.

### 4.3 Software Implementation

#### 4.3.1 PC Application

The PC application is used to read data from the data acquisition via the serial interface and to display the data. MATLAB has been selected as the programming language due to its portability and large number of libraries. MATLAB provides rich resources for data processing. Additionally, it has great flexibility, as the program can be embedded into or merged with other program easily like Excel. It is straight forward to turn the application into an internet service. For future project, a system can be developed to an online monitoring. A block diagram of the developed PC application is shown in Figure 4.11.

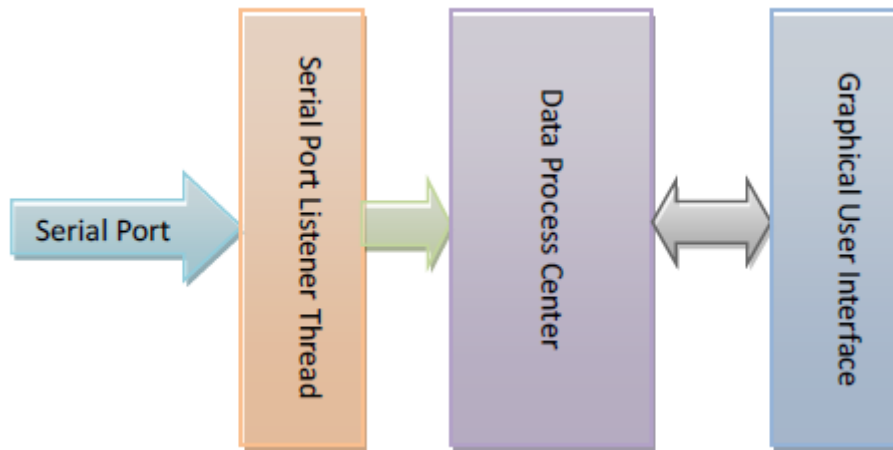


Figure 4.11 PC application diagram

The serial library is used to establish data communication between the data acquisition system and PC. The program starts a serial port listener thread to receive data from the acquisition module via the bluetooth module that appears as serial port on the PC. The received raw data are compressed into data frames. The serial listener thread decompresses these frames and decodes the data into ADC results of force sensors and digital data of magnetic rotary encoders. The program also checks the received frame and if there are errors, the error frames will not be used. Now a time series of data samples are generated based on angle and force values. These time series are displayed as the analog waveforms in the graph for force and angle values.

#### ***4.3.2 Microcontroller Application***

The microcontroller is used to communicate with sensors and send the data to personal computer via bluetooth module. Mbed library can be used for easy implementation. Implementation was made with C/C++ programming language with aid of this library.

Force sensors make communication on analog digital converter units with LPC1768's internal analog to digital converter, which use with 12-bit resolution. The resolution can be computed as follows:

$$\text{Resolution} = V_{\max} / 4096 \text{ where } V_{\max} \text{ is } 3.3\text{V} \quad (4.1)$$

According to incoming ADC values, voltage is calculated.

$$\text{Voltage} = (V_{\text{max}}/4096)*\text{ADC value} \quad (4.2)$$

The voltage results can be maximum 3.3V. The voltage values are normalized into range of 0 to 1 with software for every sensor. Touching the ground strongly gives '1' and '0' gives for foot is not touching.

Magnetic rotary encoders have communication is called as 'Serial Synchronize Interface'. It gives digital values as 10 bits. Output diagram is shown in figure 4.12.

While to make implementation, the following rules are used (OPKON Electronics, n.d.).

1. If CS<sub>n</sub> changes to logic low, Data Out (DO) will change from high impedance to logic high and the read-out will be initiated.
2. After a minimum time  $t_{\text{CLKFE}}$ , data is latched into the output shift register with the first falling edge of CLK.
3. The serial word contains 16 bits, the first 10 bits are the angular information D[9:0], the subsequent 6 bits contain system information, about the validity of data such as OCF, COF, LIN, Parity and Magnetic Field status (increase/decrease).
4. A subsequent measurement is initiated by a "high" pulse at CS<sub>n</sub> with a minimum duration of  $t_{\text{CSn}}$ .

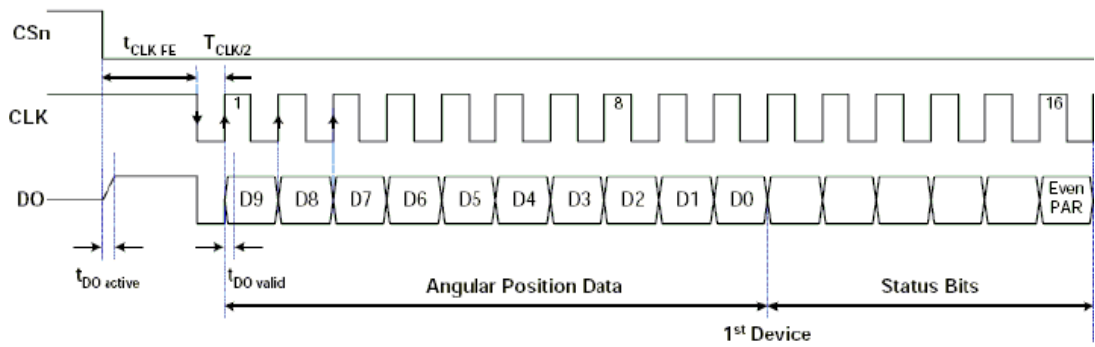


Figure 4.12 Communication protocol of encoder (OPKON Electronics, n.d.)

Finally, the obtained values from sensors to the personal computer were transferred via bluetooth device. Bluetooth makes the communication with UART pins on LPC1768 microcontroller. Computer and bluetooth is paired with a programme that is called as 'Bluesoleil' and data sets are transferred to MATLAB programme.

## CHAPTER FIVE

### SIMULATION RESULTS

#### 5.1 Introduction

In this thesis, data sets were collected for gait pattern types with data acquisition system described in chapter four. Each data set consist of either three angles (knee, hip and ankle) or ground reaction forces (toe, middle and heel). These gait patterns contain different forms of walking including ascending and descending stairs. Obtained data sets were trained with neural networks for predicting future states of joint angles and detection of gait pattern types.

Data sets were taken from a student in Dokuz Eylul University. He has physical specifications with 70 kg weight, 180 cm length and the age of 25 years old. Simulations were realized by using MATLAB program and neural network toolbox.

#### 5.2 Data Normalization

One of the most common tools used in neural networks is to take advantage of data normalization. A designer wants to have same range of values for inputs and outputs in order to minimize bias within neural network. Data normalization can speed up the training time by starting the process in same scale. There are various normalization techniques. In this thesis, min-max normalization, which is range of -1 to 1, was used. It performs linear transformation on the data. The min-max normalization formula is given in equation 5.1.

$$X'_i = (\max_{\text{target}} - \min_{\text{target}}) \cdot \left[ \frac{X_i - \min_{\text{value}}}{\max_{\text{value}} - \min_{\text{value}}} \right] + \min_{\text{target}} \quad (5.1)$$

where  $X'_i$  is new value for variable X,  $X_i$  is current value for variable X,  $X_{\min}$  is minimum value in data set and  $X_{\max}$  is maximum value in data set. Min-max normalization preserves the relationships between the original data values (Priddy, & Keller, 2005).

### 5.3 Gait Patterns

The obtained data sets were initially divided into gait cycles by means of Rancho Los Amigos Terminology and ground reaction forces. Then, these data sets were normalized with min-max normalization technique.

In this section, three figures will be given;

- i. Gait pattern types
- ii. The signals which are taken from encoders for left and right leg
- iii. The signals which are taken from force sensors into sole of shoes

Gait patterns were obtained from six walking types and named from walking pattern 1 to walking pattern 6. Every walking pattern consist of consecutive three different images.

Angle and ground reaction force data sets obtained from walking pattern types are shown in figure 5.2, 5.3, 5.4, 5.5, 5.7, 5.8, 5.9, 5.10, 5.12, 5.13, 5.15, 5.16, 5.18, 5.19, 5.21 and 5.22. In these figures, three different cycles are given in one cycle. Gait cycles obtained from walking pattern types aren't periodic and therefore, it can be seen from above given figures that there are small differences.

#### 5.3.1 Walking Pattern 1

For this walking type, two different recording were realized. One with stride length of 80 cm and step length 40 cm and the other with stride length 40 cm and step length 20 cm. Figure 5.1 shows the walking pattern 1 with stride length of 80 cm and step length of 40 cm along the walking path. In this figure,  $139 \pm 20$  samples from each sensor were taken for a single gait cycle.

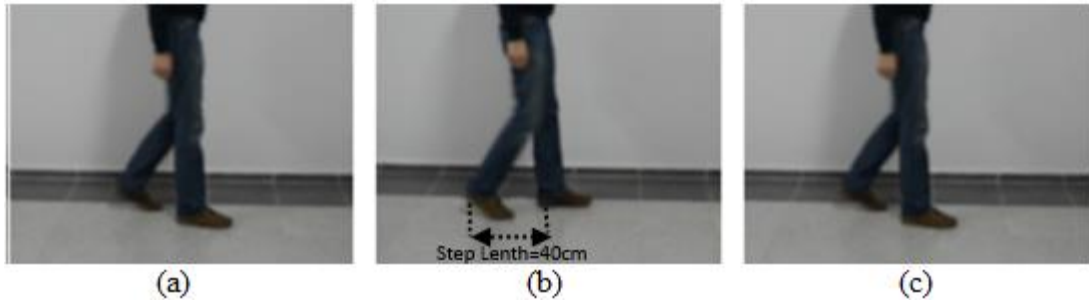


Figure 5.1 Walking pattern 1 with stride length of 80 cm and step length of 40 cm, and three consecutive images from (a) to (c)

Angle values of left and right leg joints for stride length of 80 cm and step length of 40 cm are in the range of  $0^{\circ}$  and  $360^{\circ}$ . The values are normalized to from -1 to 1. The normalized values are directly used in MATLAB neural network toolbox. After neural network processing, these normalized values are transformed back to corresponding angle values. In figure 5.2, three joints angle data values consisting of different three gait cycles are shown.

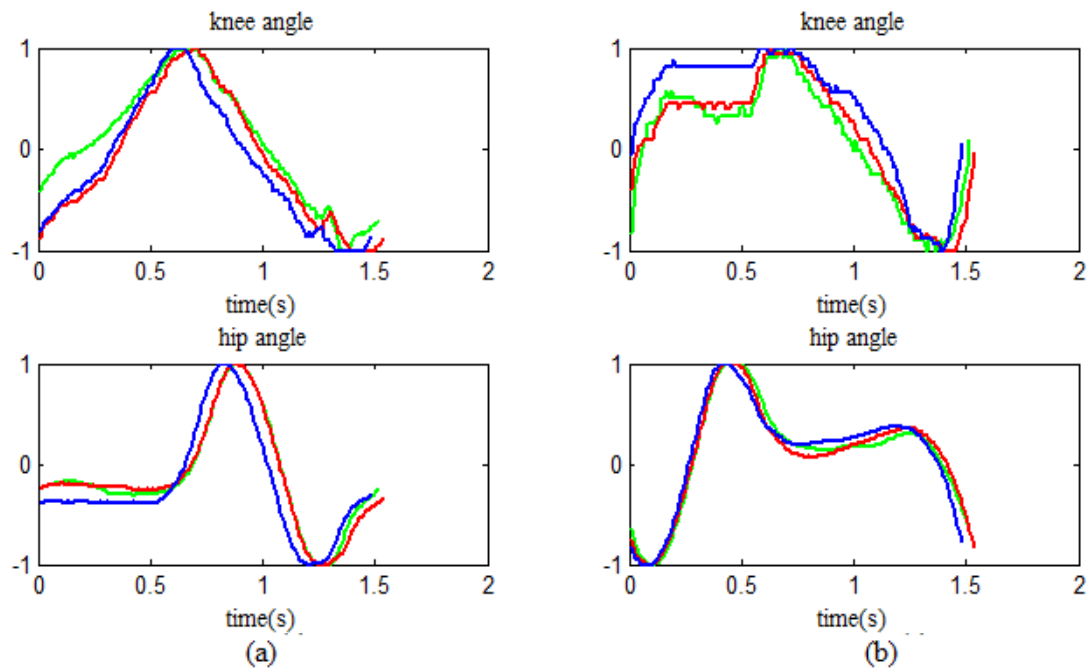


Figure 5.2 Joint angles obtained from walking pattern 1 with stride length of 80 cm and step length of 40 cm (a) Left Leg (b) Right Leg (Continue)

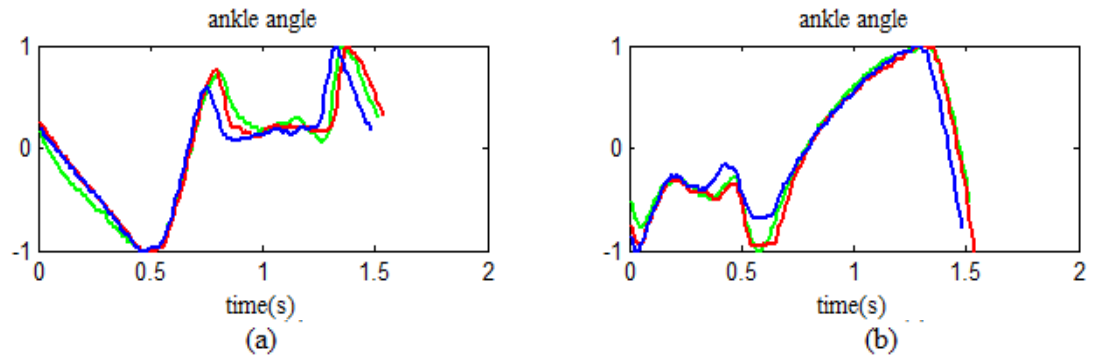


Figure 5.2 Joint angles obtained from walking pattern 1 with stride length of 80 cm and step length of 40 cm (a) Left Leg (b) Right Leg

Ground reaction force values of left and right legs for stride length of 80 cm and step length of 40 cm are in the range of 0 and 4096. The values are normalized from -1 to 1. In figure 5.3, ground reaction force data values consisting of different three gait cycles are given.

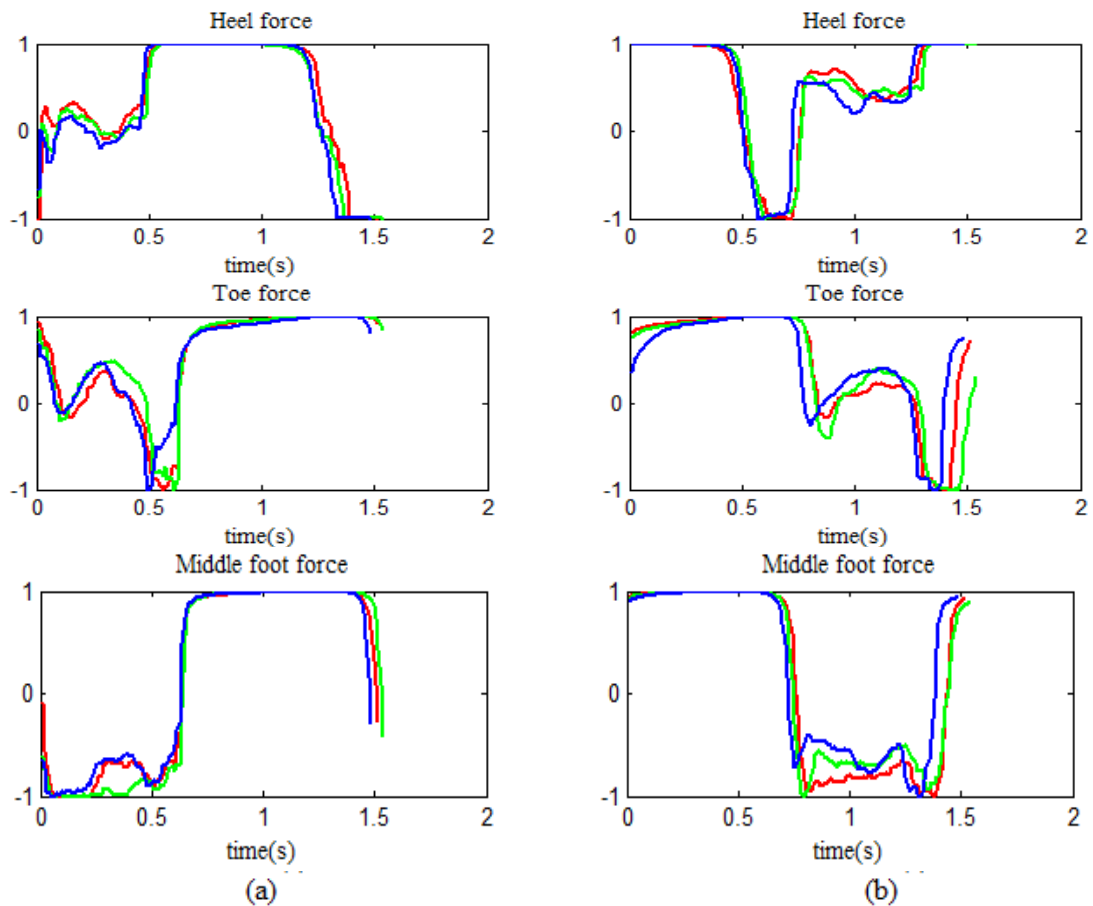


Figure 5.3 Ground reaction forces obtained from walking pattern 1 with stride length of 80 cm and step length of 40 cm (a) Right Leg (b) Left Leg

Angle values of left and right leg joints for stride length of 40 cm and step length of 20 cm are in the range of  $0^{\circ}$  and  $360^{\circ}$ . The values are normalized to from -1 to 1. In figure 5.4, three joints angle data values consisting of different three gait cycles are given.

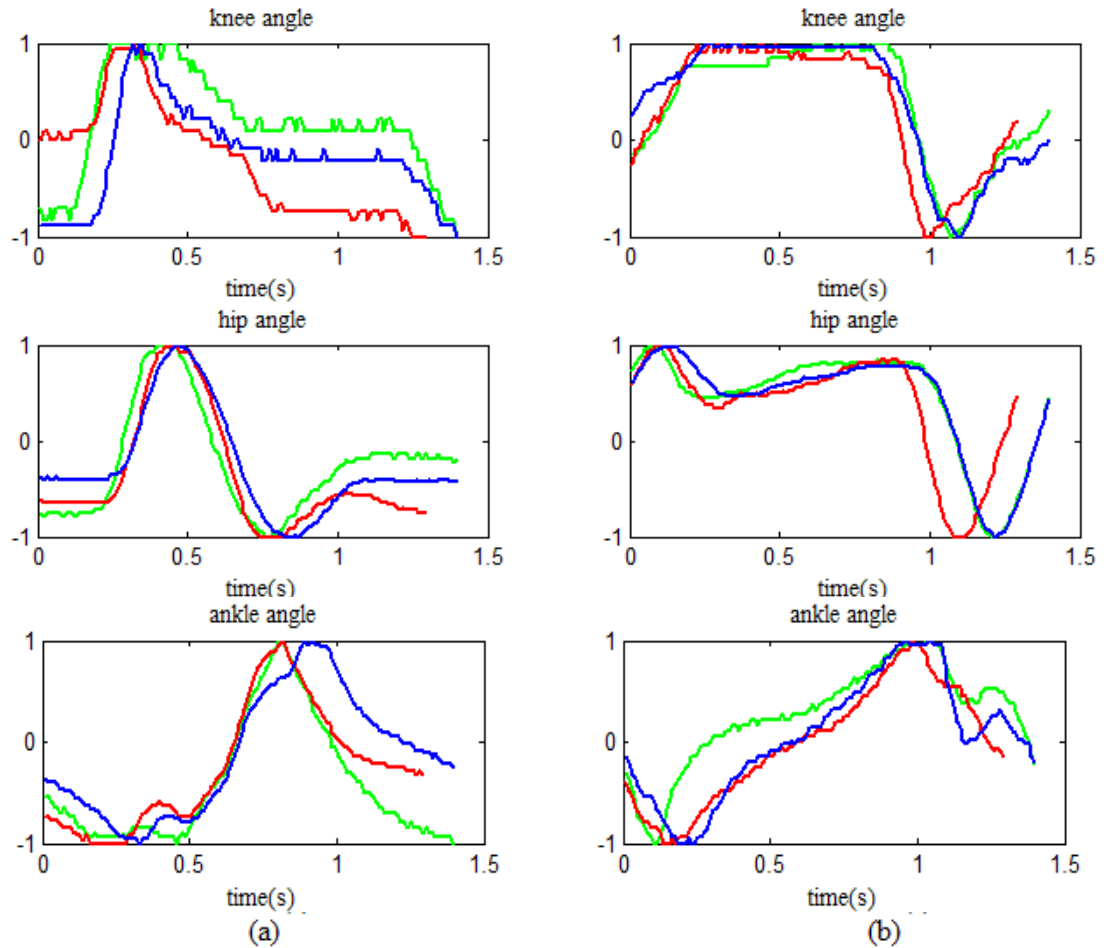


Figure 5.4 Joint angles obtained from walking pattern 1 with stride length of 40 cm and step length of 20 cm (a) Left Leg (b) Right Leg

Ground reaction force values of left and right legs for stride length of 40 cm and step length of 20 cm are in the range of 0 and 4096. The values are normalized from -1 to 1. In figure 5.5, ground reaction force data values consisting of different three gait cycles are shown.

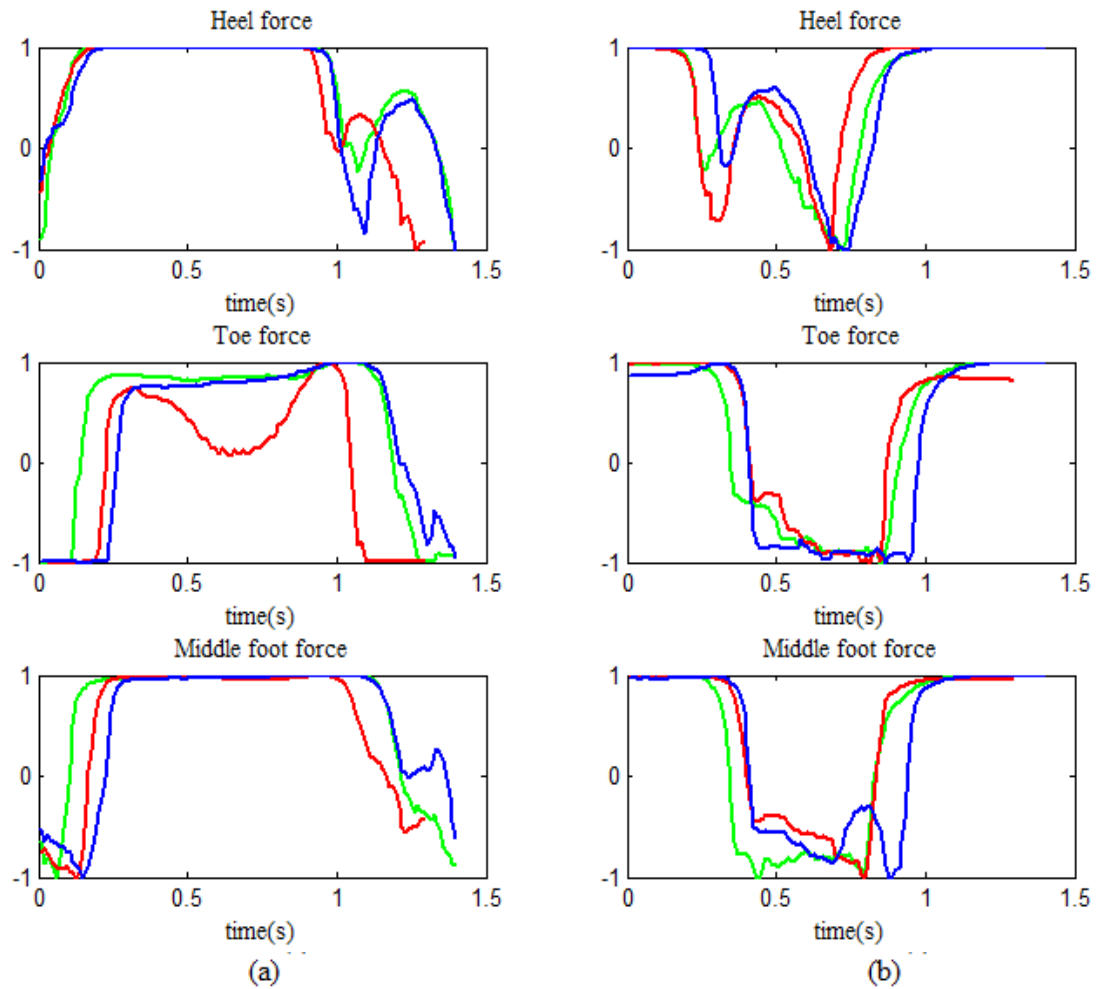


Figure 5.5 Ground reaction forces obtained from walking pattern 1 with stride length of 40 cm and step length of 20 cm (a) Right Leg (b) Left Leg

### 5.3.2 Walking Pattern 2

For this walking type, two different recording were realized. One with stride length of 80 cm and step length 40 cm and the other with stride length 40 cm and step length 20 cm. In figure 5.6, walking pattern 2 with one leg moves and then the other leg comes next to the first and then the same states. In this figure,  $154 \pm 15$  samples from each sensor were taken for single gait cycle.



Figure 5.6 Walking pattern 2 with stride length of 80 cm and step length of 40 cm, and three consecutive images from (a) to (c)

Angle values of left and right leg for stride length of 80 cm and step length of 40 cm are in the range of  $0^{\circ}$  and  $360^{\circ}$ . The values are normalized to from -1 to 1. In figure 5.7, three joints angle data values consisting of different three gait cycles belong to walking pattern 2 with 80 cm stride length are given.

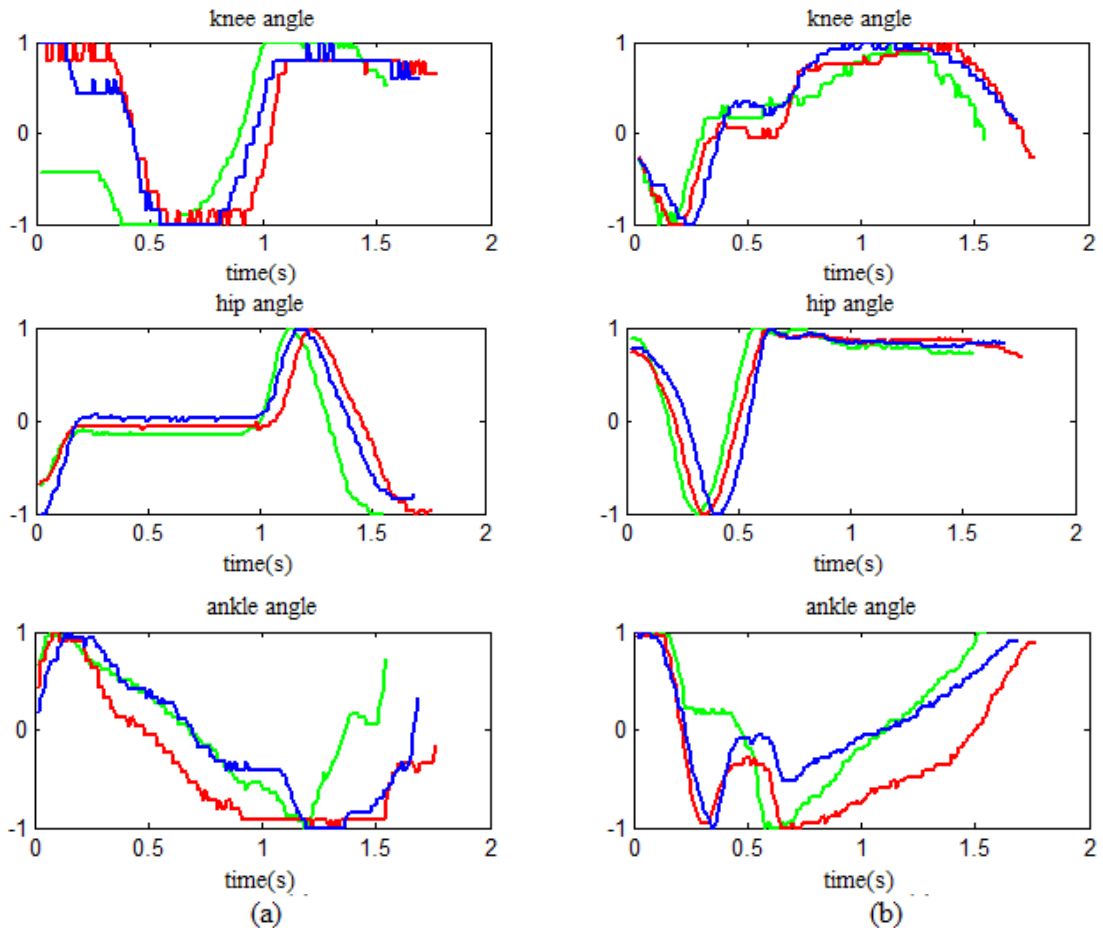


Figure 5.7 Joint angles obtained from walking pattern 2 with stride length of 80 cm and step length of 40 cm (a) Left Leg (b) Right Leg

Ground reaction force values of left and right legs for stride length of 80 cm and step length of 40 cm are in the range of 0 and 4096. The values are normalized from -1 to 1. In figure 5.8, ground reaction force data values consisting of different three gait cycles belong to walking pattern 2 with 80 cm stride length are shown.

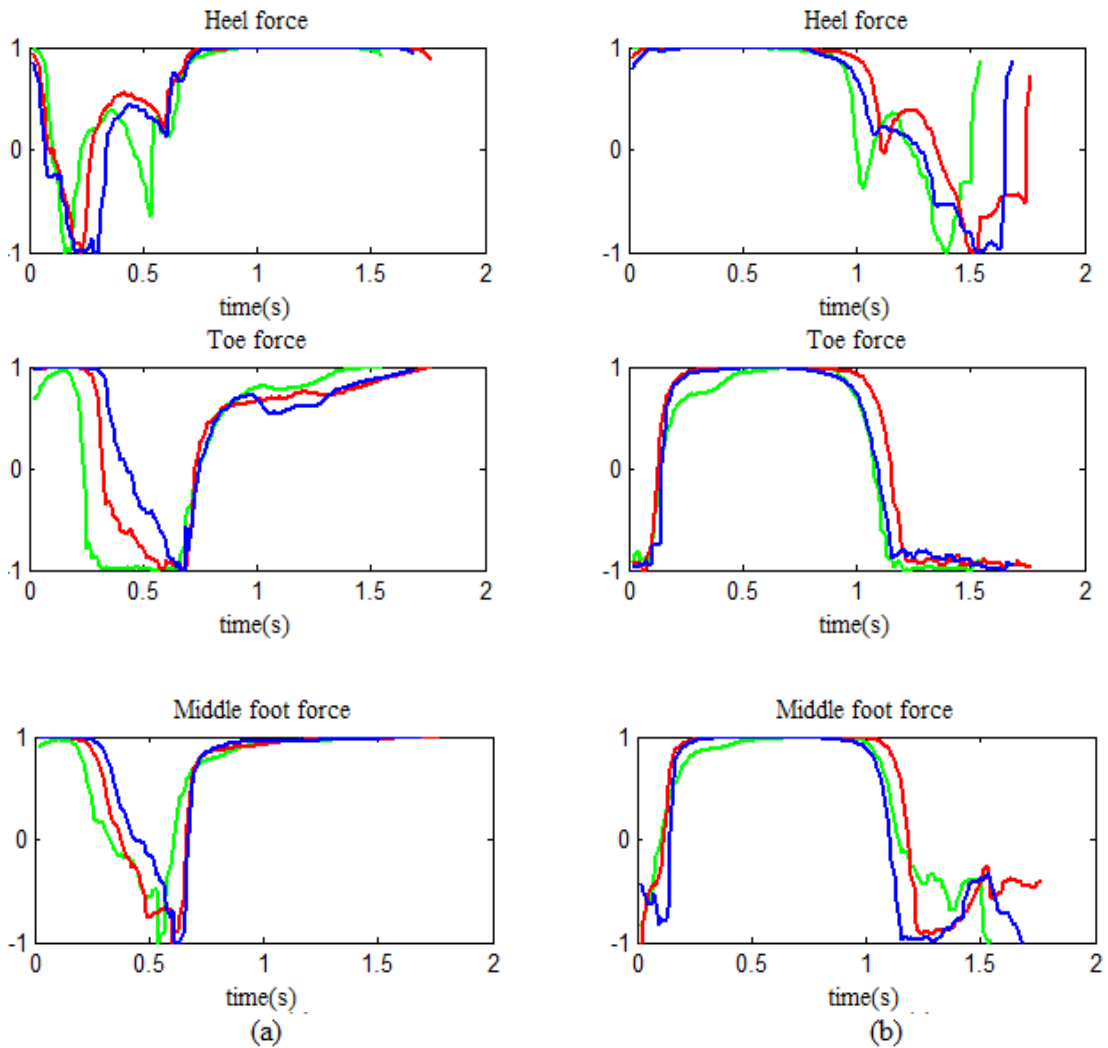


Figure 5.8 Ground reaction forces obtained from walking pattern 2 with stride length of 80 cm and step length of 40 cm (a) Right Leg (b) Left Leg

Angle values of left and right leg joints for stride length of 40 cm and step length of 20 cm are in the range of  $0^{\circ}$  and  $360^{\circ}$ . The values are normalized to from -1 to 1. In figure 5.9, three joints angle data values consisting of different three gait cycles belong to walking pattern 2 with 40 cm stride length are given.

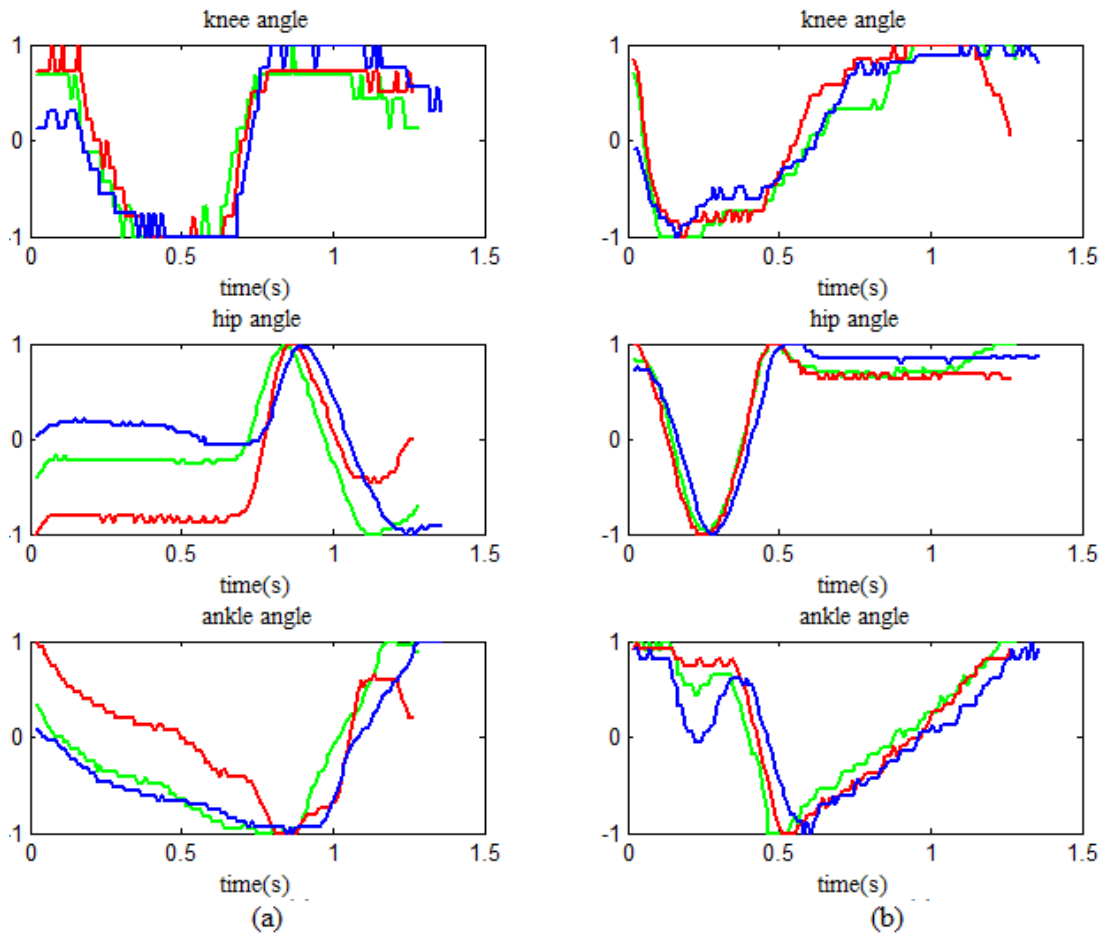


Figure 5.9 Joint angles obtained from walking pattern 2 with stride length of 40 cm and step length of 20 cm (a) Left Leg (b) Right Leg

Ground reaction force values of left and right legs for stride length of 80 cm and step length of 40 cm are in the range of 0 and 4096. The values are normalized from -1 to 1. In figure 5.10, ground reaction force data values consisting of different three gait cycles belong to walking pattern 2 with 40 cm stride length are shown.

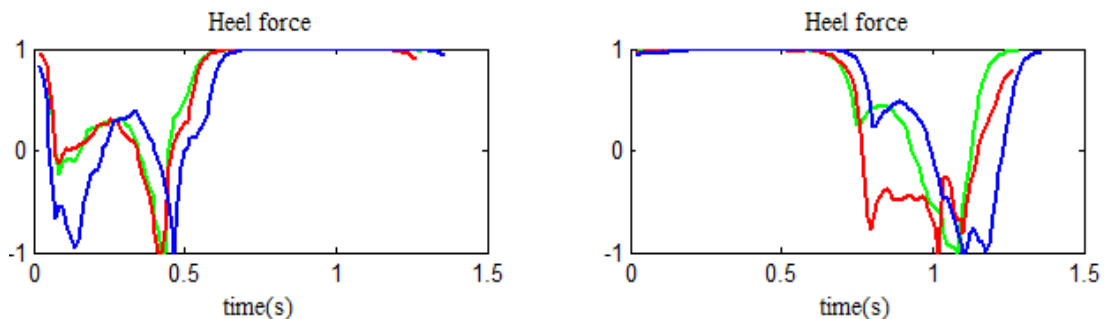


Figure 5.10 Ground reaction forces obtained from walking pattern 2 with stride length of 40 cm and step length of 20 cm (a) Right Leg (b) Left Leg (Continue)

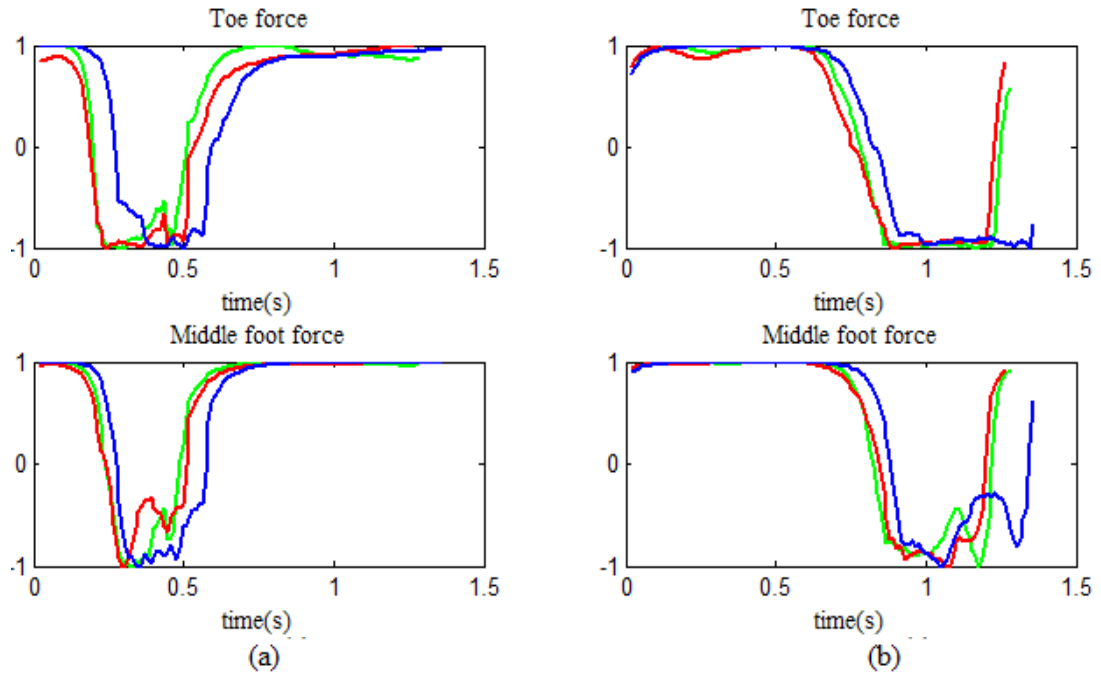


Figure 5.10 Ground reaction forces obtained from walking pattern 2 with stride length of 40 cm and step length of 20 cm (a) Right Leg (b) Left Leg

### 5.3.3 Walking Pattern 3

This walking pattern describes ascending the stairs. First, one leg moves and placed on the next stair, and then the other leg moves and placed onto the stair which is one level above other leg. This is one gait cycle and the others follow this cycle. In figure 5.11,  $209 \pm 15$  samples from each sensor were taken for a single gait cycle.



Figure 5.11 Walking pattern 3 and three consecutive images from (a) to (c)

Angle values of left and right leg joints are in the range of  $0^0$  and  $360^0$ . The values are normalized to from -1 to 1. In figure 5.12, three joints angle data values consisting of different three gait cycles belong to walking pattern 3 are given.

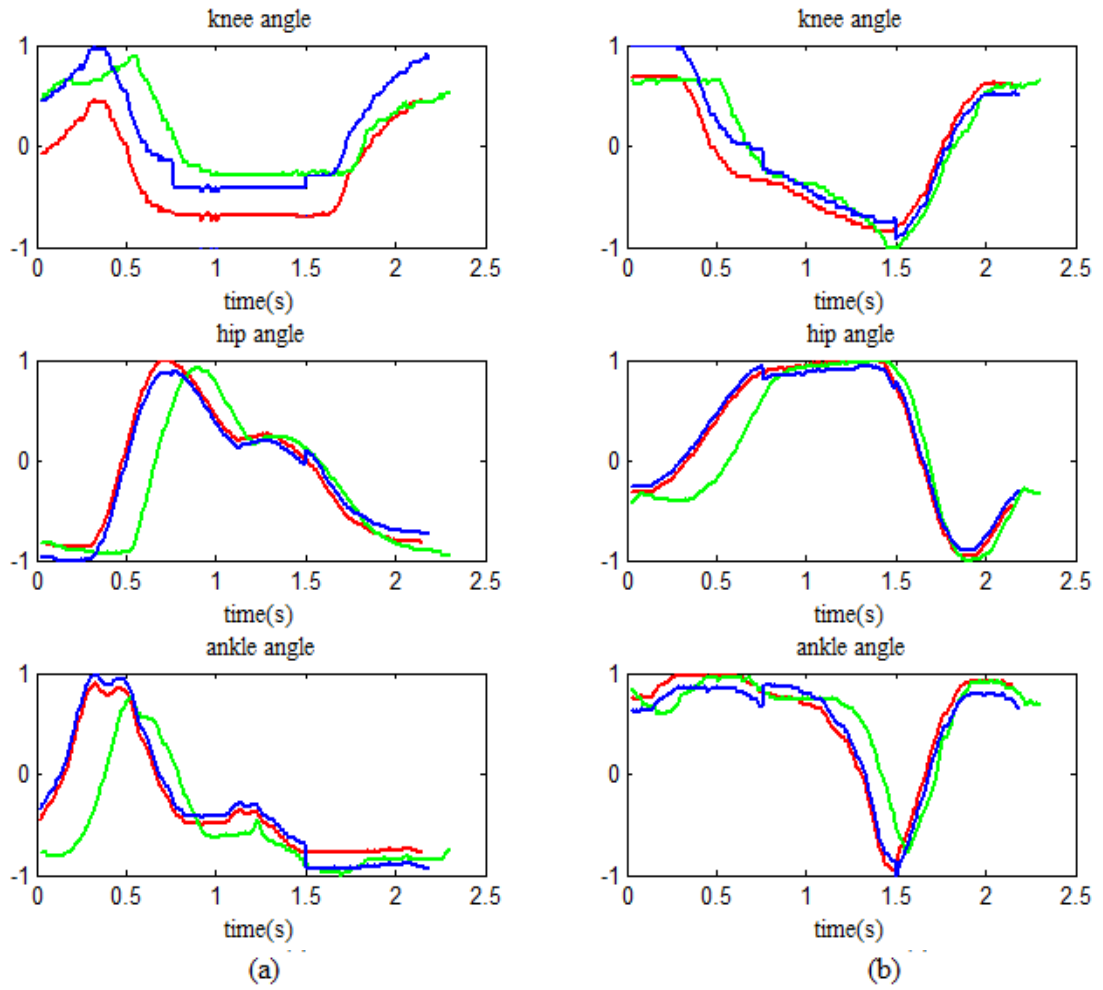


Figure 5.12 Joint angles obtained from walking pattern 3 (a) Left Leg (b) Right Leg

Ground reaction force values of left and right legs are in the range of 0 and 4096. The values are normalized from -1 to 1. In figure 5.13, ground reaction force data values consisting of different three gait cycles belong to walking pattern 3 are shown.

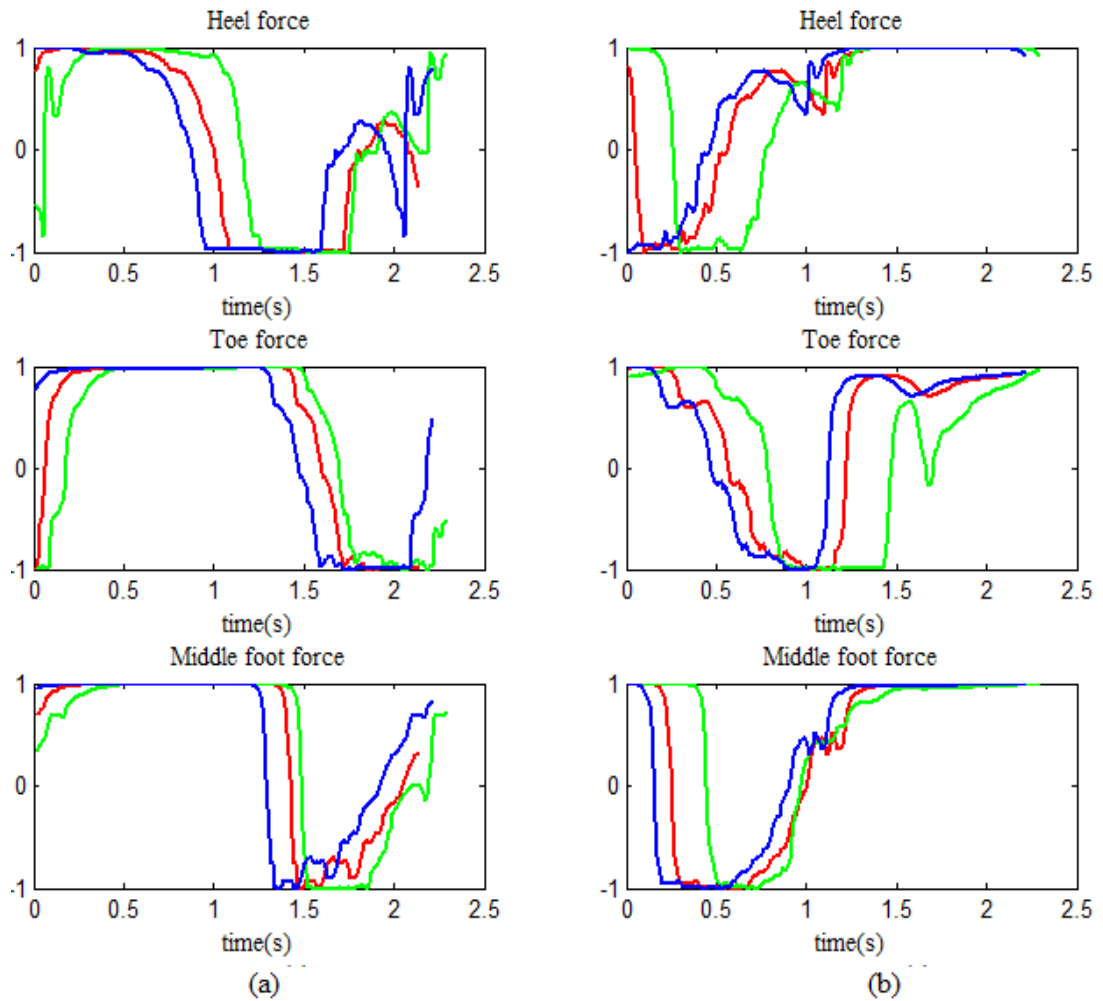


Figure 5.13 Ground reaction forces obtained from walking pattern 3 (a) Right Leg (b) Left Leg

#### 5.3.4 Walking Pattern 4

This walking pattern describes ascending the stairs. First, one leg moves and placed on the next stair, and then the other leg moves and placed onto the stair which is at the same level with the other leg. This is one gait cycle and the others follow this cycle. In figure 5.14,  $191 \pm 20$  samples from each sensor were taken for a single gait cycle.



Figure 5.14 Walking pattern 4 and three consecutive images from (a) to (c)

Angle values of left and right leg joints are in the range of  $0^0$  and  $360^0$ . The values are normalized to from -1 to 1. In figure 5.15, three joints angle data values consisting of different three gait cycles belong to walking pattern 4 are given.

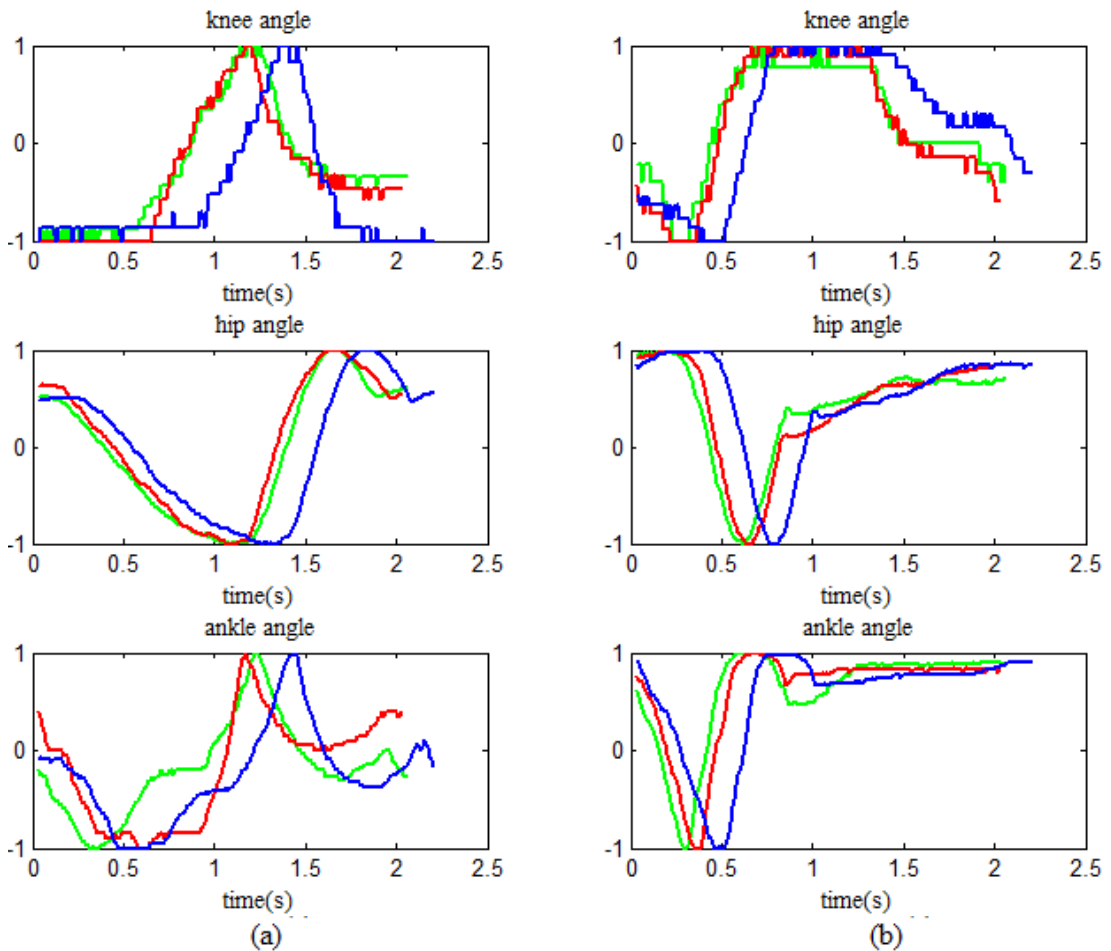


Figure 5.15 Joint angles obtained from walking pattern 4 (a) Left Leg (b) Right Leg

Ground reaction force values of left and right legs are in the range of 0 and 4096. The values are normalized from -1 to 1. In figure 5.16, ground reaction force data values consisting of different three gait cycles belong to walking pattern 4 are given.

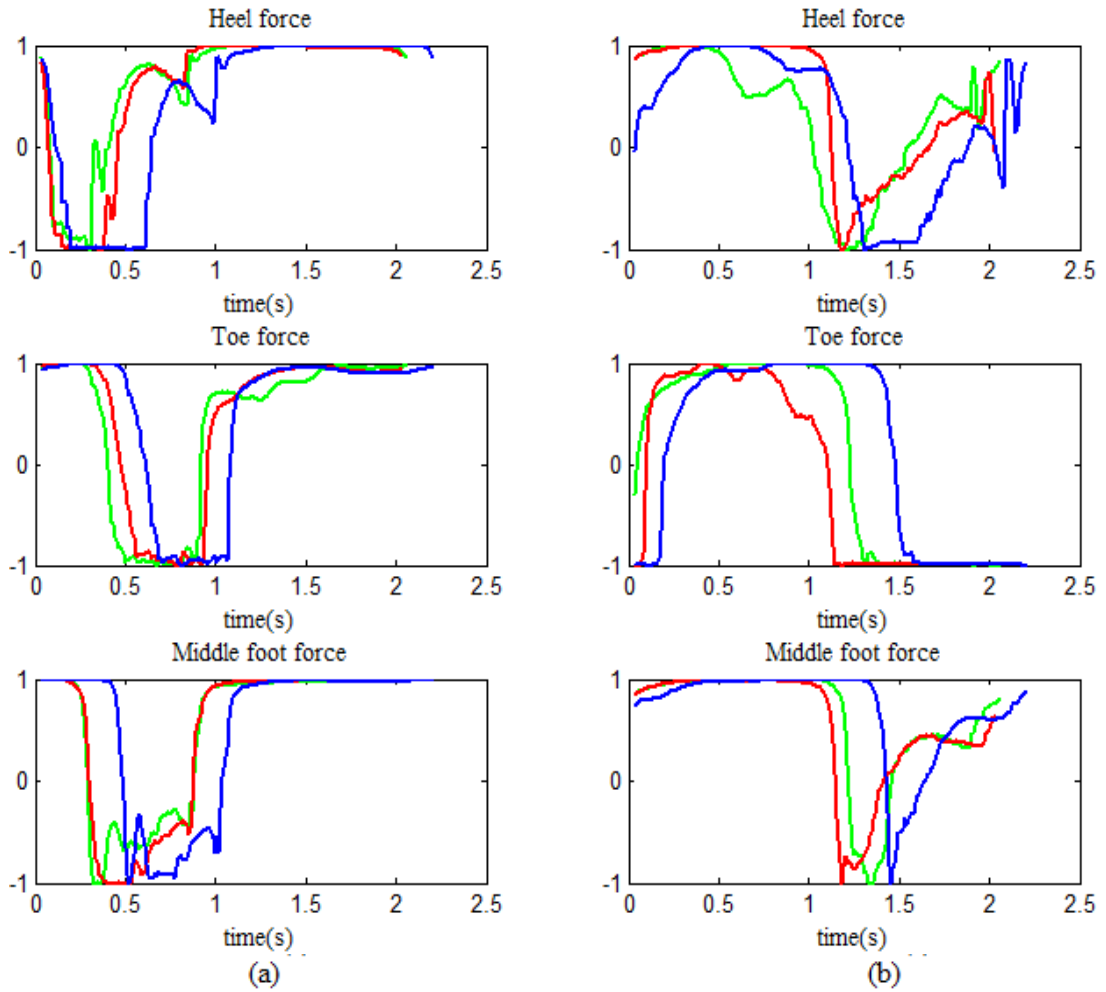


Figure 5.16 Ground reaction forces obtained from walking pattern 4 (a) Right Leg (b) Left Leg

### 5.3.5 Walking Pattern 5

This walking pattern belongs descending the stairs. First, one leg moves and placed on the next stair, and then the other leg moves and placed onto the stair which is at the same level with the other leg. This is one gait cycle and the others follow this cycle. In figure 5.14,  $195 \pm 10$  samples from each sensor were taken for a single gait cycle.



Figure 5.17 Walking pattern 5 and three consecutive images from (a) to (c)

Angle values of left and right leg joints are in the range of  $0^{\circ}$  and  $360^{\circ}$ . The values are normalized to from -1 to 1. In figure 5.18, three joints angle data values consisting of different three gait cycles belong to walking pattern 5 are given.

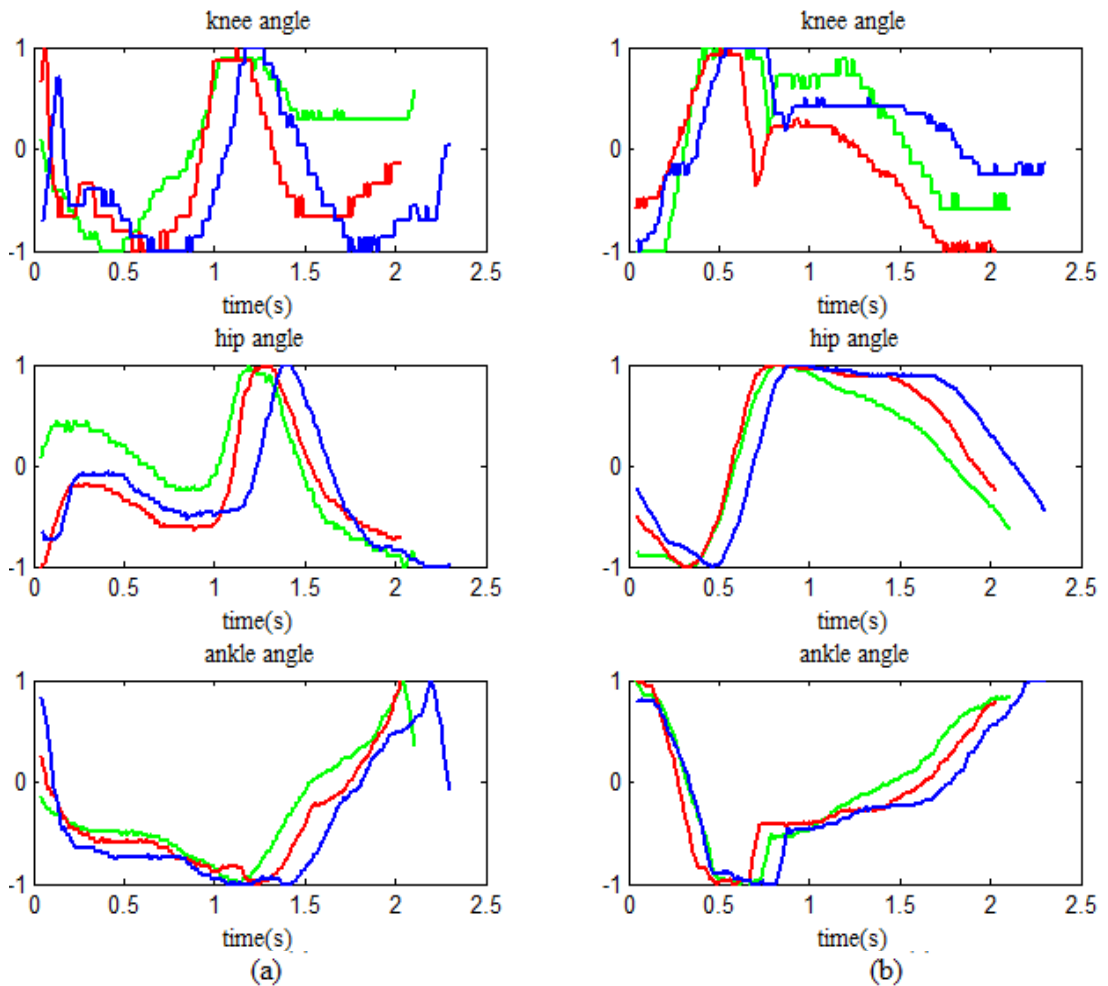


Figure 5.18 Joint angles obtained from walking pattern 5 (a) Left Leg (b) Right Leg

Ground reaction force values of left and right legs are in the range of 0 and 4096. The values are normalized from -1 to 1. In figure 5.19, ground reaction force data values consisting of different three gait cycles belong to walking pattern 5 are given.

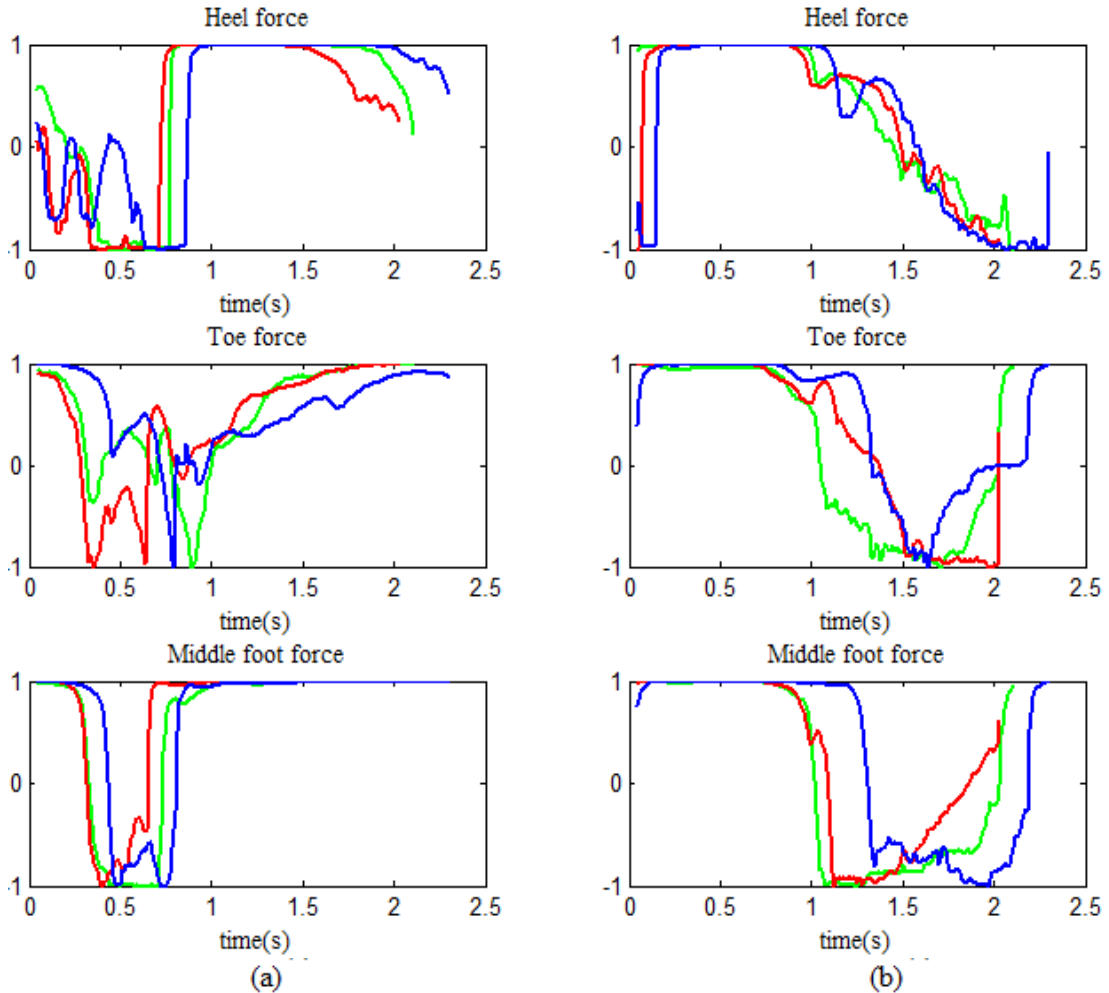


Figure 5.19 Ground reaction forces obtained from walking pattern 5 (a) Right Leg (b) Left Leg

### 5.3.6 Walking Pattern 6

This walking pattern belongs descending the stairs. First, one leg moves and placed on the next stair, and then the other leg moves and placed onto the stair which is one level below other leg. This is one gait cycle and the others follow this cycle. In figure 5.20,  $223 \pm 15$  samples from each sensor were taken for a single gait cycle.



Figure 5.20 Walking pattern 6 and three consecutive images from (a) to (c)

Angle values of left and right leg joints are in the range of  $0^{\circ}$  and  $360^{\circ}$ . The values are normalized to from -1 to 1. In figure 5.21, three joints angle data values consisting of two gait cycles are given.

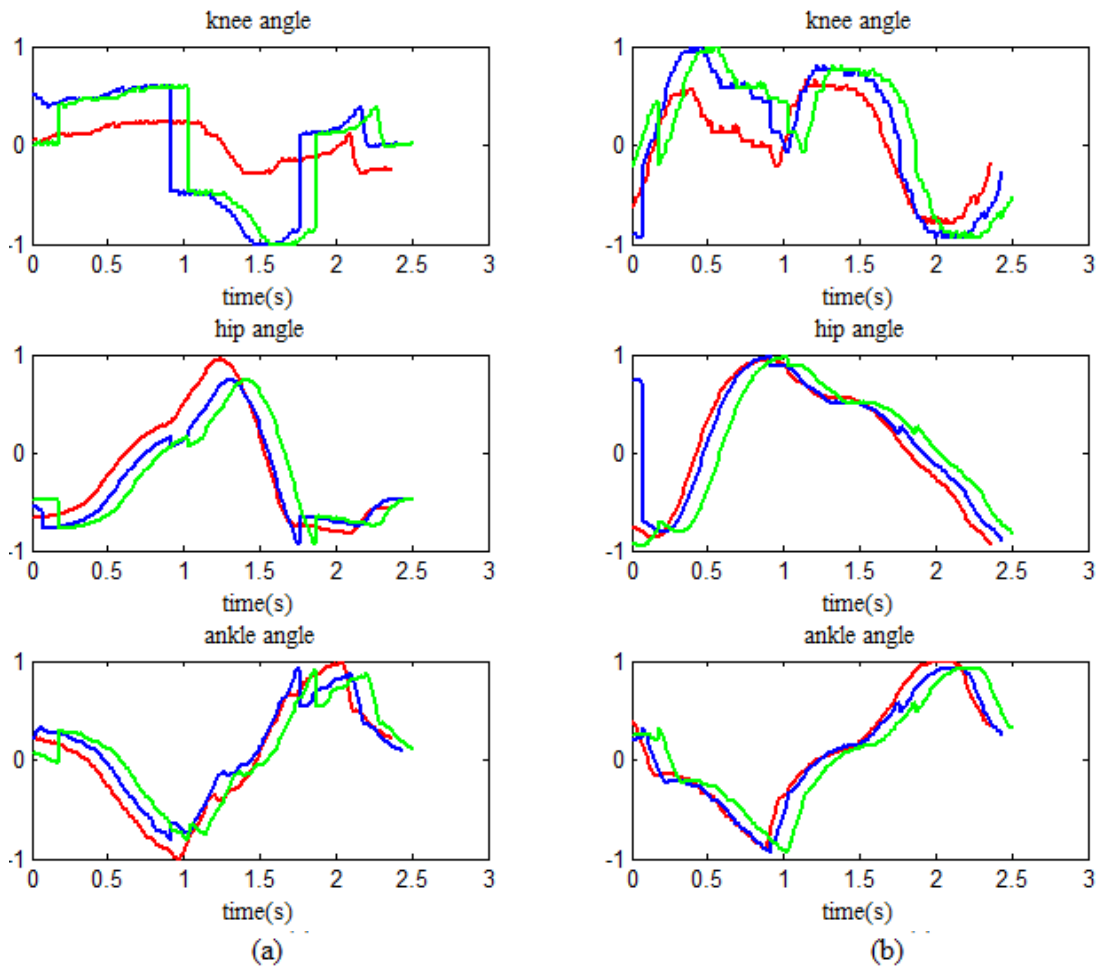


Figure 5.21 Joint angles obtained from walking pattern 6 (a) Left Leg (b) Right Leg

Ground reaction force values of left and right legs are in the range of 0 and 4096. The values are normalized from -1 to 1. In figure 5.22, ground reaction force data values consisting of two gait cycles are given.

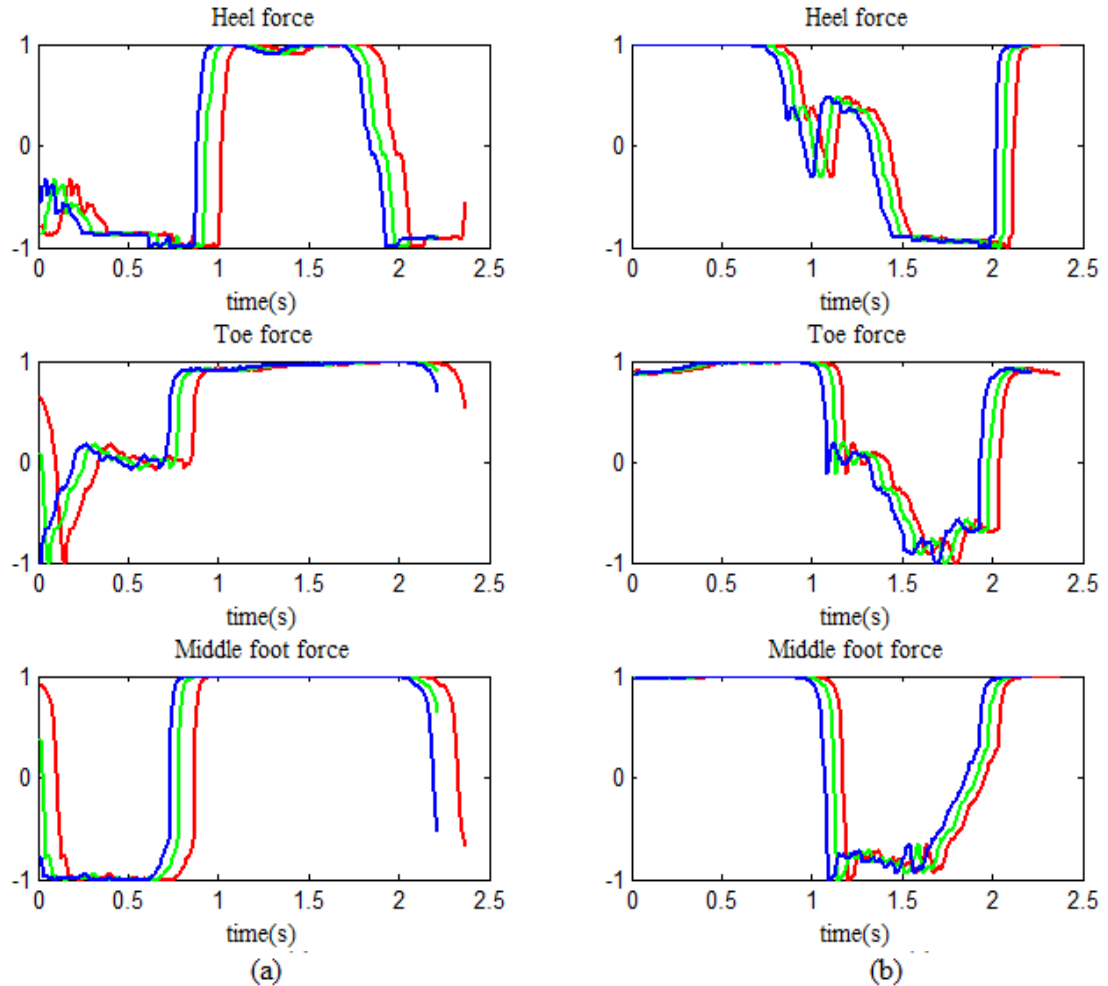


Figure 5.22 Ground reaction forces obtained from walking pattern 6 (a) Right Leg (b) Left Leg

## 5.4 Neural Network Applications

### 5.4.1 Prediction of Joint Angles

Different techniques were applied to predict future states of joint angles with neural networks. Firstly, gradient descent with momentum and Levenberg-Marquardt algorithms in MLP NN were used to train the neural network. Joint angles of right and left leg were taken as input and target respectively. Training and test of neural network were realized with single gait cycles. In table 5.1, 5.2, 5.3, 5.4, 5.5, 5.6, 5.7

and 5.8, performance analyses were given for gait pattern types. Mean square error (MSE) and absolute percentage error parameters were used to compare performances.

MSE is computed with formula in equation 5.2 (Wackerly, & Scheaffer, 2008).

$$MSE = \frac{1}{n} \sum_{i=1}^n (\text{Target} - \text{Output})^2 \quad (5.2)$$

Mean absolute percentage error is calculated with formula in equation 5.3 (Yamin, & Shahidehpour, 2010).

$$\text{Percentage Error} = \frac{|\text{Approximate Value} - \text{Exact Value}|}{|\text{Exact Value}|} \times \frac{100\%}{n} \quad (5.3)$$

where n is number of data.

Table 5.1 Performance comparisons of LM and GDM backpropagation algorithms for walking pattern 1 with stride length of 80 cm and step length of 40 cm

	Training Data		Test Data	
	MSE	Error Rate	MSE	Error Rate
LM	0.0367	0.0221%	114.91	2.31%
GDM	0.3572	0.1399%	62.7285	1.69%

Table 5.2 Performance comparisons of LM and GDM backpropagation algorithms for walking pattern 1 with stride length of 40 cm and step length of 20 cm

	Training Data		Test Data	
	MSE	Error Rate	MSE	Error Rate
LM	0.0114	0.0084%	98.5887	1.86%
GDM	1.2764	0.2649%	46.6118	1.18%

Table 5.3 Performance comparisons of LM and GDM backpropagation algorithms for walking pattern 2 with stride length of 80 cm and step length of 40 cm

	Training Data		Test Data	
	MSE	Error Rate	MSE	Error Rate
LM	0.0782	0.0326%	52.9061	1.62%
GDM	0.3911	0.1501%	39.7325	1.14%

Table 5.4 Performance comparisons of LM and GDM backpropagation algorithms for walking pattern 2 with stride length of 40 cm and step length of 20 cm

	Training Data		Test Data	
	MSE	Error Rate	MSE	Error Rate
LM	0.0719	0.035%	30.56	1.30%
GDM	0.2753	0.127%	23.433	1.14%

Table 5.5 Performance comparisons of LM and GDM backpropagation algorithms for walking pattern 3

	Training Data		Test Data	
	MSE	Error Rate	MSE	Error Rate
LM	0.0144	0.02%	95.63	2.12%
GDM	1.5215	0.29%	18.90	0.99%

Table 5.6 Performance comparisons of LM and GDM backpropagation algorithms for walking pattern 4

	Training Data		Test Data	
	MSE	Error Rate	MSE	Error Rate
LM	0.1698	0.04%	30.17	1.28%
GDM	0.5548	0.16%	14.56	0.78%

Table 5.7 Performance comparisons of LM and GDM backpropagation algorithms for walking pattern 5

	Training Data		Test Data	
	MSE	Error Rate	MSE	Error Rate
LM	0.1625	0.05%	387.31	4.58%
GDM	2.7549	0.37%	393.02	4.41%

Table 5.8 Performance comparisons of LM and GDM backpropagation algorithms for walking pattern 6

	Training Data		Test Data	
	MSE	Error Rate	MSE	Error Rate
LM	0.1751	0.06%	559.3	5.49%
GDM	2.7275	0.37%	426.3	4.4%

The results have shown that Levenberg-Marquardt algorithm is more successful than gradient descent with momentum algorithm to train the neural network. Despite getting better results for training, it has worse results when given test data. It can be told that best training performance isn't be able to give better response.

Secondly, ground reaction force values obtained from sensors placed into soles of right leg added to joint angles to generate wider input data set. Gradient descent with momentum algorithm in MLP NN was used to train neural networks because it has

given better results for test data sets in previous study. In table 5.9, 5.10, 5.11, 5.12, 5.13, 5.14, 5.15 and 5.16, performance analyses depending on input data set are given for all of the gait pattern types.

Table 5.9 Performance comparisons of neural networks depending on input data set for walking pattern 1 with stride length of 80 cm and step length of 40 cm

Input Data Set	Training Data		Test Data	
	MSE	Error Rate	MSE	Error Rate
Angle	0.3572	0.1399%	62.7285	1.69%
Angle-Force	1.1844	0.24%	29.80	0.98%

Table 5.10 Performance comparisons of neural networks depending on input data set for walking pattern 1 with stride length of 40 cm and step length of 20 cm

Input Data Set	Training Data		Test Data	
	MSE	Error Rate	MSE	Error Rate
Angle	1.2764	0.2649%	46.6118	1.18%
Angle-Force	0.6634	0.18%	58.27	1.36%

Table 5.11 Performance comparisons of neural networks depending on input data set for walking pattern 2 with stride length of 80 cm and step length of 40 cm

Input Data Set	Training Data		Test Data	
	MSE	Error Rate	MSE	Error Rate
Angle	0.3911	0.1501%	39.7325	1.14%
Angle-Force	0.2604	0.11%	23.17	0.87%

Table 5.12 Performance comparisons of neural networks depending on input data set for walking pattern 2 with stride length of 40 cm and step length of 20 cm

Input Data Set	Training Data		Test Data	
	MSE	Error Rate	MSE	Error Rate
Angle	0.2753	0.127%	23.433	1.14%
Angle-Force	0.2715	0.11%	18.86	0.93%

Table 5.13 Performance comparisons of neural networks depending on input data set for walking pattern 3

Input Data Set	Training Data		Test Data	
	MSE	Error Rate	MSE	Error Rate
Angle	1.5215	0.29%	18.90	0.99%
Angle-Force	1.7487	0.28%	16.55	0.97%

Table 5.14 Performance comparisons of neural networks depending on input data set for walking pattern 4

Input Data Set	Training Data		Test Data	
	MSE	Error Rate	MSE	Error Rate
Angle	0.5548	0.16%	14.56	0.78%
Angle-Force	0.5309	0.15%	10.5	0.76%

Table 5.15 Performance comparisons of neural networks depending on input data set for walking pattern 5

Input Data Set	Training Data		Test Data	
	MSE	Error Rate	MSE	Error Rate
Angle	2.7549	0.37%	393.02	4.41%
Angle-Force	1.4294	0.29%	236.81	3.21%

Table 5.16 Performance comparisons of neural networks depending on input data set for walking pattern 6

Input Data Set	Training Data		Test Data	
	MSE	Error Rate	MSE	Error Rate
Angle	2.7275	0.37%	426.3	4.4%
Angle-Force	2.62	0.38%	272.97	3.22%

Obtained results have shown that ground reaction forces improve both training and test performance of neural network.

Thirdly, MLP NN, RBF NN and RNN were applied to training neural networks. Joint angles and ground reaction forces of right leg were taken as input data set because wider training input data set provided better results as shown in previous study. Joint angles of left leg were taken as target. Performance comparisons of neural networks were given in table 5.17, 5.18, 5.19, 5.20, 5.21, 5.22, 5.23 and 5.24.

Table 5.17 Performance comparisons of multilayer perceptrons, radial basis function and Elman recurrent neural networks for walking pattern 1 with stride length of 80 cm and step length of 40 cm

ANN Model	Training Data		Test Data	
	MSE	Error Rate	MSE	Error Rate
MLP NN	1.1844	0.24%	29.80	0.98%
RBF NN	0.0658	0.06%	28.52	0.95%
Elman RNN	0.5698	0.16%	15.10	0.96%

Table 5.18 Performance comparisons of multilayer perceptrons, radial basis function and Elman recurrent neural networks for walking pattern 1 with stride length of 40 cm and step length of 20 cm

ANN Model	Training Data		Test Data	
	MSE	Error Rate	MSE	Error Rate
MLP NN	0.6634	0.18%	58.27	1.36%
RBF NN	0.0993	0.07%	91.76	1.76%
Elman RNN	0.3342	0.13%	42.27	1.28%

Table 5.19 Performance comparisons of multilayer perceptrons, radial basis function and Elman recurrent neural networks for walking pattern 2 with stride length of 40 cm and step length of 20 cm

ANN Model	Training Data		Test Data	
	MSE	Error Rate	MSE	Error Rate
MLP NN	0.2715	0.11%	18.86	0.93%
RBF NN	0.0377	0.04%	13.005	0.79%
Elman RNN	0.2140	0.21%	33.24	1.17%

Table 5.20 Performance comparisons of multilayer perceptrons, radial basis function and Elman recurrent neural networks for walking pattern 2 with stride length of 80 cm and step length of 40 cm

ANN Model	Training Data		Test Data	
	MSE	Error Rate	MSE	Error Rate
MLP NN	0.2604	0.11%	23.17	0.87%
RBF NN	0.0902	0.06%	404.61	3.91%
Elman RNN	0.1258	0.08%	11.50	0.78%

Table 5.21 Performance comparisons of multilayer perceptrons, radial basis function and Elman recurrent neural networks for walking pattern 3

ANN Model	Training Data		Test Data	
	MSE	Error Rate	MSE	Error Rate
MLP NN	1.7487	0.28%	16.55	0.97%
RBF NN	0.0828	0.07%	41.48	1.44%
Elman RNN	3.008	0.38%	30.26	1.29%

Table 5.22 Performance comparisons of multilayer perceptrons, radial basis function and Elman recurrent neural networks for walking pattern 4

ANN Model	Training Data		Test Data	
	MSE	Error Rate	MSE	Error Rate
MLP NN	0.5309	0.15%	10.5	0.76%
RBF NN	0.0911	0.06%	10.26	0.73%
Elman RNN	0.2091	0.09%	31.05	1.31%

Table 5.23 Performance comparisons of multilayer perceptrons, radial basis function and Elman recurrent neural networks for walking pattern 5

ANN Model	Training Data		Test Data	
	MSE	Error Rate	MSE	Error Rate
MLP NN	1.4294	0.29%	236.81	3.21%
RBF NN	0.3816	0.14%	311.92	4.48%
Elman RNN	1.2954	0.26%	273.39	3.17%

Table 5.24 Performance comparisons of multilayer perceptrons, radial basis function and Elman recurrent neural networks for walking pattern 6 with stride length of 40 cm and step length of 20 cm

ANN Model	Training Data		Test Data	
	MSE	Error Rate	MSE	Error Rate
MLP NN	2.62	0.38%	272.97	3.22%
RBF NN	1.09	0.22%	216.2	3.63%
Elman RNN	1.52	0.28%	197.6	3%

It can be seen that RBF NN gives worse performance than MLP NN and RNN when given test data although it has the best training performance for each gait pattern type. It can be said again that the best training performance doesn't always give better result as shown in previous study.

Fourthly, instead of single gait cycle, two and three gait cycle data sets were used to train neural networks. Joint angles and ground reaction forces of right leg were taken as input data set. Joint angles of left leg were taken as target. Recurrent neural network were chosen for training. Neural network were tested with single gait cycle data sets. In table 5.25, 5.26, 5.27, 5.28, 5.29, 5.30, 5.31 and 5.32, performance comparisons are given depending on number of gait cycle for gait pattern types.

Table 5.25 Performance comparisons of neural networks depend on number of gait cycles used in training for walking pattern 1 with stride length of 80 cm and step length of 40 cm

	<b>Training Data</b>	<b>Test Data</b>
<b>No of Cycles</b>	<b>Error Rate</b>	<b>Error Rate</b>
1	0.16%	0.96%
2	0.25%	0.77%
3	0.48%	0.76%

Table 5.26 Performance comparisons of neural networks depend on number of gait cycles used in training for walking pattern 1 with stride length of 40 cm and step length of 20 cm

	<b>Training Data</b>	<b>Test Data</b>
<b>No of Cycles</b>	<b>Error Rate</b>	<b>Error Rate</b>
1	0.13%	1.28%
2	0.25%	0.84%
3	0.42%	0.73%

Table 5.27 Performance comparisons of neural networks depend on number of gait cycles used in training for walking pattern 2 with stride length of 80 cm and step length of 40 cm

	<b>Training Data</b>	<b>Test Data</b>
<b>No of Cycles</b>	<b>Error Rate</b>	<b>Error Rate</b>
1	0.21%	1.17%
2	0.31%	0.92%
3	0.24%	0.88%

Table 5.28 Performance comparisons of neural networks depend on number of gait cycles used in training for walking pattern 2 with stride length of 40 cm and step length of 20 cm

	<b>Training Data</b>	<b>Test Data</b>
<b>No of Cycles</b>	<b>Error Rate</b>	<b>Error Rate</b>
1	0.08%	0.78%
2	0.11%	0.66%
3	0.15%	0.57%

Table 5.29 Performance comparisons of neural networks depend on number of gait cycles used in training for walking pattern 3

	<b>Training Data</b>	<b>Test Data</b>
<b>No of Cycles</b>	<b>Error Rate</b>	<b>Error Rate</b>
1	0.38%	1.29%
2	0.22%	0.6%
3	0.29%	0.58%

Table 5.30 Performance comparisons of neural networks depend on number of gait cycles used in training for walking pattern 4

	<b>Training Data</b>	<b>Test Data</b>
<b>No of Cycles</b>	<b>Error Rate</b>	<b>Error Rate</b>
1	0.09%	1.31%
2	0.14%	0.69%
3	0.18%	0.68%

Table 5.31 Performance comparisons of neural networks depend on number of gait cycles used in training for walking pattern 5

	<b>Training Data</b>	<b>Test Data</b>
<b>No of Cycles</b>	<b>Error Rate</b>	<b>Error Rate</b>
1	0.26%	3.17%
2	0.46%	3.13%
3	0.57%	3.04%

Table 5.32 Performance comparisons of neural networks depend on number of gait cycles used in training for walking pattern 6

	<b>Training Data</b>	<b>Test Data</b>
<b>No of Cycles</b>	<b>Error Rate</b>	<b>Error Rate</b>
1	0.28%	3.0%
2	0.82%	2.89%
3	1.1%	2.41%

It has shown that performances of neural networks were increased proportionally depending on number of gait cycles.

### 5.4.2 Detection of Gait Pattern Types

In this study, learning vector quantization (LVQ) neural networks were applied to detect gait pattern types; walking type 1 with stride length of 40 cm and step length of 20 cm, walking pattern type 2 with stride length of 40 cm and step length of 20 cm, walking pattern 4 in figure 5.14 and walking pattern 5 in figure 5.17. Joint angles and ground reaction forces were normalized between -1 and 1. These normalized values were used in MATLAB neural network toolbox.

Firstly, 100 joint angle data sets obtained from right and left leg were used to teach gait pattern types to neural networks. Neural networks were trained with 40, 50 and 60 neurons. In table 5.33, training performances are given depending on the number of neuron in the hidden layer. Mean square error (MSE) and error rate parameters were used to compare network performances.

Table 5.33 Training performance comparisons depending on the number of neuron in the hidden layer and angle input data set

Number of Neuron	MSE	Error Rate
40	0.257	51.49%
50	0.260	52%
60	0.264	51.79%

100 joint angle data sets were used to test the neural network. In table 5.34, performance analyses of neural networks were given depending on the number of neurons.

Table 5.34 Success rate of LVQ NN for test data sets consist from joint angles

Number of Neuron	Success Rate
40	50.31%
50	50.39%
60	50.58%

The results have shown that neural networks could detect only two types of the gait patterns with joint angles with angle data sets. The number of neurons less than

40, the neural network had 25% success rate and it has reached to saturation performance level after 60 neurons.

Secondly, 100 ground reaction force data set obtained from sensors into sole of right leg added to angle values to train the neural networks with wider training data set. Neural networks were trained with different number of neuron; 10, 20, 30, 40. In table 5.35, performances of neural networks were given depending on number of neuron for training process.

Table 5.35 Training performance comparisons depending on the number of neurons in the hidden layer and combination of input data sets

Number of Neuron	MSE	Error Rate
10	0.105	21.03%
20	0.114	23.79%
30	0.101	20.2%
40	0.103	20.5%

100 test data sets were used to test neural networks. In table 5.36, performance analyses were given depending on number of neuron.

Table 5.36 Success rate of LVQ NN for test data sets consist from combination of input data sets

Number of Neuron	Success Rate
10	75.57%
20	73.2%
30	75.2%
40	75.57%

Results has shown that neural networks could detect the gait patterns more successfully with wider training data set, which consist of joint angles and ground reaction forces. Neural network performance have reached to saturation level with 30 neurons and its success rate obtained approximately 75%.

In addition to LVQ NN, MLP NN was also used to detect these four types of gait patterns. Input data sets were taken as joint angles and ground reaction forces of right

leg and corresponding four outputs were taken as 1, 2, 3 and 4. Neural network was trained for different hidden layer neuron numbers. The neural network with 10 neurons in the hidden layer had better performance than others. The network produces outputs in the range of 0-1.5, 1.51-2.5, 2.51-3.5 and 3.51-4.5 for the test patterns 1, 2, 4, and 5, respectively. In table 5.37, performance analysis of the neural network is shown.

Table 5.37 Success rate of MLP NN for detection of four types of gait patterns

<b>Walking Pattern 1</b>	<b>Walking Pattern 2</b>	<b>Walking Pattern 4</b>	<b>Walking 5</b>
75.1%	88.7%	84.23%	79.51%

Results have shown that MLP NN could detect the four types of gait patterns more successfully than LVQ. It gives 81.885% average success rate.

LVQ and MLP NN were used to detect for two types of gait patterns, walking pattern 1 with stride length of 80 cm and step length of 40 cm and walking pattern 4. Ground reaction forces and joint angles of right leg were chosen as input data values. Targets were taken as 1 and 2 for walking pattern 4 and walking pattern 1, respectively. The neural networks were trained with these data sets. The network gives output values in the range of 0.4 to 1.5 for test pattern 4 and 1.5 to 2.0 for test pattern 1. Therefore, a threshold value for MLP NN was taken as 1.5. In addition to MLP NN, LVQ algorithm determines the threshold value automatically. In table 5.38 and 5.39, performance analysis of neural networks are shown.

Table 5.38 Success rate of MLP NN for detection of two types of gait patterns

<b>Walking Pattern 1</b>	<b>Walking Pattern 4</b>
100%	99.26%

Table 5.39 Success rate of LVQ NN for detection of two types of gait patterns

<b>Walking Pattern 1</b>	<b>Walking Pattern 4</b>
100%	86.84%

## **CHAPTER SIX**

### **CONCLUSIONS AND FUTURE WORK**

In this thesis, artificial neural networks were used to predict gait angles and gait patterns. To predict gait angles and gait pattern types artificial neural networks were trained with data sets obtained from joint angles or both joint angles and ground reaction forces. For both cases various type and size of artificial neural networks were trained to provide performance comparison.

The collected data has shown that knee, hip and ankle angles have different values for each gait pattern type. The collected data had some minor errors because of possible inaccurate placement of sensors and mechanical design structure. These errors have been neglected throughout the study. However, because of nature of the generalization of ANN, these errors have been eliminated. The data were taken from a subject with a weight of 70 kilograms and 25 years old.

Different trials were applied to predict the future states of three joints angles. Firstly, gradient descent with momentum (GDM) and Levenberg-Marquardt (LM) algorithms for MLP NN were used to train neural networks. For this only angle values were chosen as input data set. Training and test data sets were taken for one gait cycle. The results have shown that Levenberg-Marquardt training algorithm is more successful than gradient descent with momentum training algorithm. Despite getting better results for training process, gradient descent with momentum algorithm has provided better response for the test data. It can be said that better training doesn't always mean better decision system.

Secondly, ground reaction forces obtained from sensors placed into shoe sole were added to angle values to generate wider training data set. GDM algorithm was used to train the system since it has previously given better response. Obtained results have shown that ground reaction forces improve the performance for both training and test processes.

Thirdly, neural networks consist of MLP NN, RBF NN and RNN, were applied to compare which one has the best performance. Training set which include joint angles and ground reaction forces was chosen because of getting better performance. The best training performance have been taken with RBF NN for every gait pattern. However, RBF NN has given the worst performance than others for the given a test data. It can be said again that the best training performance doesn't mean the best network.

Finally, training data sets with two and three gait cycles instead of only one gait cycle were used to train the neural network. Training performance was slightly deteriorated depending on the number of gait cycles. The more gait cycles is used the worst performance is obtained. Because of dissimilarities between the gait cycles, it becomes difficult to provide less training error. However, because of generalization, the performance of neural network for test data sets increased proportionally.

In this study, neural networks were also used to detect gait pattern types including ascend and descend the stair. Firstly, Training and test processes were realized with different input data sets and different number of neurons in the hidden layer for four types of gait patterns. The test results have shown that neural networks with input data consist of joint angles and ground reaction forces had better performance and required less number of neurons in the hidden layer. In comparison to 50% success rate of the LVQ NN with only angle inputs, LVQ NN with angle and ground reaction force input provided approximately 75% success rate. In addition to LVQ NN, MLP NN gives 81.885% average success rate. Then, the neural networks were trained for detection of two types of walking patterns. The results has shown that the LVQ neural network had 93.42% average success rate and MLP NN had 99.63% average success rate depending on test data sets.

Consequently as a future work, this project can be expanded by adding various portable sensors; accelerometers, gyro sensors and EMG sensors. Moreover, gait patterns covering running, sit down and up on a chair can be analyzed with neural networks. Performances of different artificial intelligent systems like fuzzy systems

and genetic algorithms can also be examined. Furthermore, studies can be increased on detection of abnormal gait patterns and determination of gait phases.

## REFERENCES

- Baker, R. (2006). Gait analysis methods in rehabilitation. *Journal of neuroengineering and rehabilitation*, 3, 1-10.
- Bamberg, S.J.M., Benbasat, A.Y., Scarborough, D.M., Krebs, D.E., & Paradiso, J.A. (2008). Gait analysis using a shoe-integrated wireless sensor system. *IEEE Transactions on Information Technology in Biomedicine*, 12 (4), 413–423.
- Barton, J.G., & Lees, A. (1995). An application of neural networks for distinguishing gait patterns on the basis of hip-knee joint angle diagrams. *Gait & Posture*, 5, 28-33.
- Betker, A., Maharjan, P., Yaduvanshi, C., Szturm, T., & Moussavi, Z. (2008). Automated quantification and comparison of spatio-temporal gait parameters during treadmill and overground walking. *Proceeding of IEEE Electrical and Computer Engineering*, 165-168.
- Capi, G., Nasu, Y., Barolli, L., & Mitobe, K. (2002). Real time gait generation for autonomous humanoid robots: A case study for walking. *Robotics and Autonomous Systems Journal*, 42 (2), 107-116.
- Chakraborty, R.C. (2007). *Fundamentals of neural network: Soft computing*. Retrieved January 21, 2014, from [http://www.myreaders.info/02-Fundamentals\\_of\\_Neural\\_Network.pdf](http://www.myreaders.info/02-Fundamentals_of_Neural_Network.pdf).
- Core Electronics (n.d.). *Core electronics user guide: JY-MCU Bluetooth to UART wireless serial port module for Arduino*. Retrieved January 21, 2014, from <https://core-electronics.com.au/store/attachments/guides/Product-User-Guide-JYMCU -Bluetooth-UART-R1-0.pdf>.

- Cuccurallo, S.J. (2010). *Physical medicine and rehabilitation board review* (2<sup>nd</sup> ed.). NY: Demos medical publishing.
- Djuric-Jovicic, M.D., Jovicic, N.S., & Popovic, D.B. (2011). Kinematics of gait: A new method for angle estimation based on accelerometers. *Sensors*, *11*, 10571-10585.
- Dorofki, M., Elshafie, A.H., Jaafar, O., Karim, O.A, & Mastura, S. (2012). Comparison of artificial neural network transfer functions abilities to simulate extreme run off data. *International Proceedings of Chemical, Biological and Environmental Engineering*, *33*, 39-44.
- Dreeben-Irimie, O. (2011). *Introduction to physical therapy for physical therapist assistants* (2<sup>nd</sup> Ed.). USA: Jones & Bartlett Learning.
- Fröchlich, J. (1996). *Neural networks with java*. Retrieved January 21, 2014 from <http://fbim.fh-regensburg.de/~saj39122/jfroehl/diplom/e-index.html>.
- Gabel, M., Gilad-Bachrach, R., Renshaw, E., & Schuster, A. (2012). Full body gait analysis with kinect. *IEEE Engineering in Medicine and Biology Society*, *34*, 1964-1967.
- Galushkin, A. (2007). *Neural networks theory*. Berlin: Springer-Verlag.
- Gökcegöz, F. (2013). *STM8S – HC06 bluetooth modül ile haberleşme uygulamaları*. Retrieved January 21, 2014, from <http://www.mcu-turkey.com/tag/hc-06-bluetooth-module/>.
- Hagan, M., Demuth, H.B., & Beale, M. (1996). *Neural network design*. USA: PWS.
- Haykin, S. (2005). *Neural networks: A comprehensive foundation* (9th Ed.). India: Pearson Education.

- Interlink Electronics (2010). *Force sensing resistors: Integration guide*. Retrieved January 21, 2014, from [http://www.digikey.com/Web%20Export/Supplier%20Content/InterlinkElectronics\\_1027/PDF/Interlink\\_Electronics\\_Integration\\_Guide.pdf?redirected=1](http://www.digikey.com/Web%20Export/Supplier%20Content/InterlinkElectronics_1027/PDF/Interlink_Electronics_Integration_Guide.pdf?redirected=1).
- Kirtley, C. (2006). *Clinical gait analysis*. China: Elsevier Churchill Livingstone.
- Kong, K., & Tomizuka, M. (2008). Estimation of abnormalities in a human gait using sensor embedded shoes. *Proceedings of the 2008 IEEE International Conference on Advanced Intelligent Mechatronics*, 1331-1336.
- Kutilek, P., & Farkasova, B. (2011). Prediction of lower extremities' movement by angle-angle diagrams and neural network. *Acta of Bioengineering and Biomechanics*, 13 (2), 57-65.
- Kwon, D.Y., & Gross, M. (2005). Combining body sensors and visual sensors for motion training. In *Proceedings of the 2005 Association for Computing Machinery Special Interest Group on Computer-Human Interaction International Conference on Advances in Computer Entertainment Technology*, 94–101.
- Lippert, L.S. (2011). *Clinical kinesiology and anatomy*. USA: F.A. Davis Company.
- Mandic, D.P., & Chambers, J.A. (2001). *Recurrent neural networks for prediction: Learning algorithms, architectures, and stability*. NY: John Wiley & Sons.
- NXP Semiconductors (2009). *Rapid prototyping for the LPC1768 MCU*. Retrieved January 21, 2014, from <http://www.nxp.com/documents/leaflet/LPC1768.pdf>.
- OPKON Electronics (n.d.). *Absolute encoder with serial communication*. Retrieved January 21, 2014, from [http://www.opkon.com.tr/pdf/MRA%2050\\_Ver.101011.pdf](http://www.opkon.com.tr/pdf/MRA%2050_Ver.101011.pdf).

- Pappas, I.P.I, Popovic, M.R., Keller, T., Dietz, V., & Morari, M. (2001). A reliable gait phase detection system. *IEEE Transactions on Neural Systems and Rehabilitation Engineering*, 9 (2), 113-125.
- Pawin, J., Khaorapapong, T., & Chawalit, S. (2011). Neural-based human's abnormal gait detection using force sensitive resistors. *Fourth International Workshop on Advanced Computational Intelligence*, 19-21.
- Perry, J. (1992). *Gait analysis: Normal and pathological function*. New Jersey: SLACK.
- Pham, D.T. & Liu, X. (1995). *Neural networks for identification, prediction and control*. London: Springer-Verlag.
- Pinitlertsakun, J., & Charoensuk, W. (2012). Knee angle prediction during stair ascending gait of trans-femoral amputee. *The 2012 Biomedical Engineering International Conference*, 1-5.
- Priddy, K.L., & Keller, P.E. (2005). *Neural networks: An introduction*. Washington: SPIE.
- Pulliam, C.L., Lambrecht, J.M., & Kirsch, R.F. (2011). EMG-based neural network control of transhumeral Prostheses. *Journal of Rehabilitation Research & Development*, 48 (6), 739-754.
- Rana, N.K. (2009). Application of force sensing resistor (FSR) in design of pressure scanning system for plantar pressure measurement. *International Conference on Computer and Electrical Engineering*, 234, 678-685.
- Rojas, R. (1996). *Neural networks: A systematic introduction*. Berlin: Springer-Verlag.

- Sant'Anna, A., Wickström, N., Eklund, H., & Tranberg, R. (2012). A wearable gait analysis system using inertial sensors Part II: Evaluation in a clinical setting. *Proceedings of the International Conference on Bio-Inspired Systems and Signal Processing*, 5-14.
- Sparkfun (n.d.). *Force sensitive resistor – square*. Retrieved January 21, 2014, from <https://www.sparkfun.com/products/9376>.
- Tao, W., Liu, T., Zheng, R., & Feng, H. (2012). Gait analysis using wearable sensors. *Sensors*, 12, 2255-2283.
- Teixido, M., Palleja, T., Tresanchez, M., Nogues, M., & Palacin, J. (2011). Measuring oscillating walking paths with a LIDAR, *Sensor*, 11, 5071-5076.
- Touzed, C. (n.d.). *Les reseaux de neurones artificiels*. Retrieved January 21, 2014, from [http://e-philo.univ-paris1.fr/TP1\\_CONX.htm](http://e-philo.univ-paris1.fr/TP1_CONX.htm).
- Toygar, E.M., Özkurt, A., Kırıl, Z., Çakmakçı, M., Gören Kırıl, B., Şenol, Y., et al. (2012). İnsan bacak hareketleri için prototip dış iskelet robotik sisteminin mekanik tasarımı ve hareket verilerinin yapay sinir ağları ile elde edilmesi. *Sakarya Üniversitesi Fen Bilimleri Enstitüsü Dergisi*, 16 (3), 234-248.
- Vaughan, C.L., Davis, B.L., & O'connor, J.C. (1999). *Dynamics of human gait* (2nd Ed.). Cape Town: Kiboho.
- Wackerly, D., & Scheaffer, W. (2008). *Mathematical Statistics with Applications* (7 ed.). USA: Thomson Higher Education.
- Wahab, Y., Bakar, N.A. (2011). Gait analysis measurement for sport application based on ultrasonic system. *In Proceeding of the IEEE 15th International Symposium on Consumer Electronics*, 20-24.

Wang, L., & Buchanan, T. (2002). Prediction of joint moments using a neural network model of muscle activations from EMG signals. *IEEE Transactions on Neural Systems and Rehabilitation Engineering*, 10 (1), 30-37.

Whittle, M. (2007). *Gait analysis: An introduction*. Oxford: Butterworth – Heinemann.

Yamin, H.Y., & Shahidehpour, S.M. (2010). Bidding strategies using price based unit commitment in a deregulated power market. *Electric Power Components and Systems*, 32 (3), 229-245.